CHAPTER 5

RESULTS AND DISCUSSION

The 2-dimensional compressible Navier-Stokes equations are solved for all the configurations as discussed in the section 4.4.1 through computational fluid dynamics techniques using the ANSYS FLUENT 14.5. The current study focuses on the shock-shock interactions for the design of efficient biplane configurations which can successfully avoid or reduce the effect of flow chocking for the Busemann biplane at lower Mach numbers ($M_\infty \leq 1.7$). The multi-block method is used for the grid generation for all the geometries. The concept of stagger has been tested in this investigation as a means to reduce the flow chocking with reduced wave drag at lower Mach numbers. Additionally, as the sharp leading and trailing edges discussed in the literature is not feasible from manufacturing point of view and also from structural stability point of view, the effect of leading and trailing edge radii on the shock-shock interactions for the staggered and non-staggered Busemann biplane configurations are presented here. All the investigations are done at angles of attack varying between zero to 4° angles of attack.

5.1 Busemann biplane with Stagger Configuration at $\alpha = 0^o$

Although the Busemann biplane shows decent performance near the design freestream Mach number of 1.7, high wave drag occurs when the Mach number is less than 1.7. As any aircraft has to start from subsonic velocities and accelerate through all intermediate Mach numbers, the Busemann biplane needs to be redesigned so that the high drag at lower Mach numbers zone caused by the choked-flow phenomenon can be avoided or at least reduced. Staggering of the biplane elements has been proposed as a means to avoid the choking at supersonic

Mach numbers below the design speed. If the ratio of throat area to inlet area A_t/A_i of a biplane is large, it becomes startable at a lower supersonic Mach numbers. The larger the area ratio of the section area of the inlet to that of the throat is, the easier it is to avoid chocking. Apart from increasing the minimum area between the planes, the staggering of the planes makes the bow shock wave to be attached with the leading element, hence reducing the stagnation pressures and accompanying wave drag.

The increase in the amount of stagger x, increases the throat to inlet area of the biplane configuration. The inlet to throat area for different staggered configuration is given in Table 5.1.

Table 5.1: Ratios of throat to inlet area.

x	0	0.1 c	0.2 c	0.3 c	0.4 c	0.5 c
A_t/A_i	0.800	0.84	0.88	0.92	0.96	1.000

The thickness to chord ratio for all the staggered configurations of the Busemann airfoils are t/c = 0.05 for each element. The vertical distance between the staggered elements, i.e. the gap is set to 0.5, so that the results can easily be compared with the standard Busemann and diamond airfoils. The number of grids and the solution method and the physical models that were validated for the Busemann biplane and the diamond airfoils are used to obtain solution for flow around all geometric configurations.

In case of Busemann biplane the pressure distribution between the elements is symmetrical about centerline and hence provides the zero lift at zero degree angle of attack. For the staggered configurations at subsonic speeds, the flow continues to expand due to friction in the constant area of the throat resulting reduced surface pressure ahead of the point of maximum thickness on both the lower and upper element as shown in Fig 5.1. This reduction in pressure not only results in reduced drag at subsonic Mach numbers but the increased suction on lower element provides a small amount of lift as well.

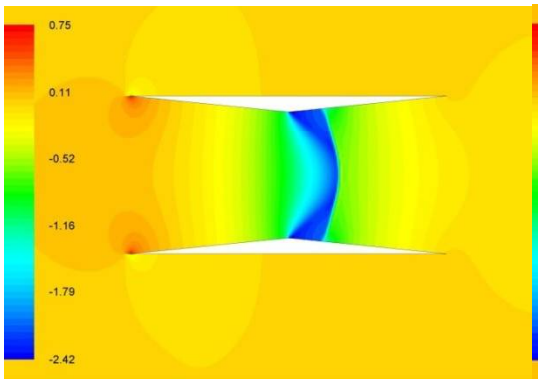

Busemann Biplane

(C_D = 0.0168, C_L = 0.0000)

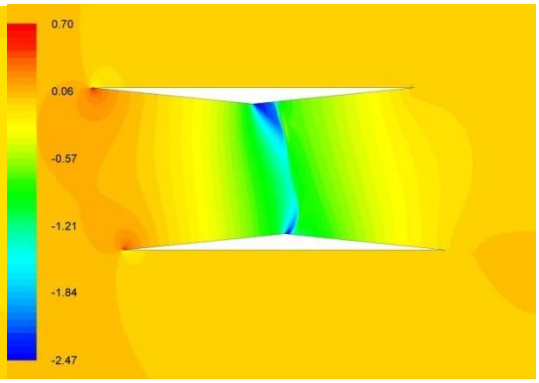

Stagger Upper Element 0.1c

(C_D = 0.0185, C_L = 0.0439)

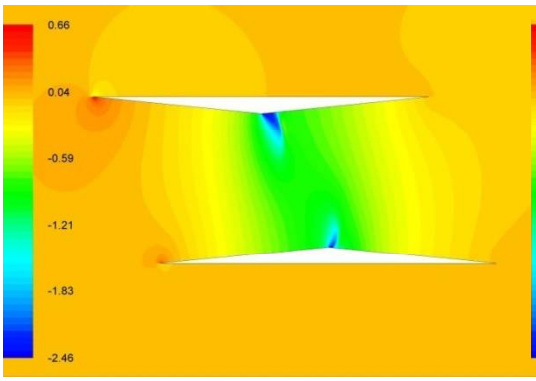

Stagger 0.2c

(C_D = 0.0438, c_l = 0.0231)

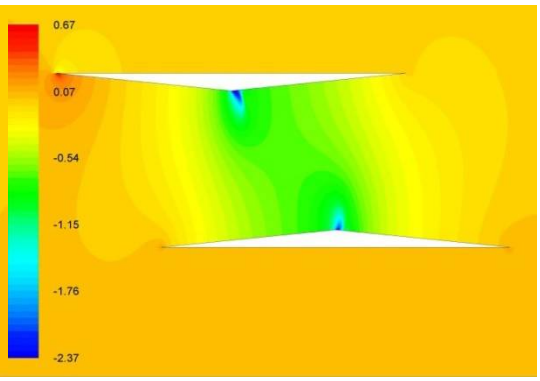

Stagger 0.3c

(C_D = 0.1117, C_L = 0.1296)

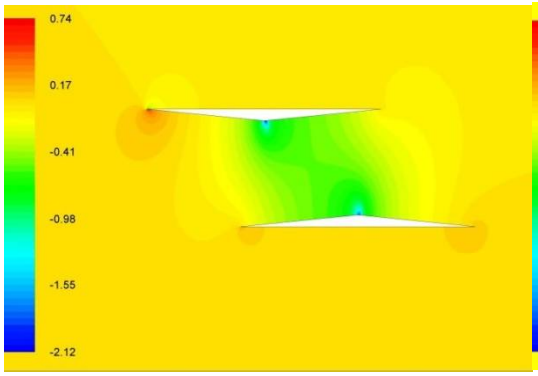

Stagger 0.4c

(C_D = 0.0172, c_l = 0.1652)

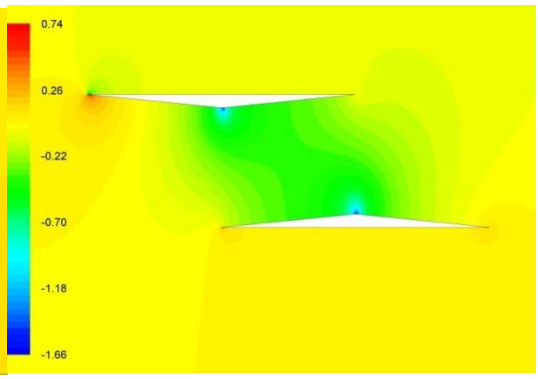

Stagger 0.5c

(C_D = 0.0170, C_L = 0.1909)

Fig. 5.1: Pressure Variation with Stagger distance at M_∞ = 0.6 and α = 0°

With an increase in the stagger at subsonic speeds, the pressure distributions become more favorable with associated increase in lift and reduction in drag. The contours of pressure for the different staggered configuration at a supersonic freestream Mach number of 1.6 is shown in Fig. 5.2. It clearly shows that for a stagger of 0.1c, the strength of the bow shock wave ahead of the body is decreases as the shock wave becomes slightly oblique due to the shifting of lower element backwards. Despite an increase in the throat area due to staggering the flow remains choked for a stagger of 0.1c and a marginal reduction from 0.0992 to 0.0949, in the drag is observed. The flow symmetry about the centre line is lost and a small lift force is seen to act due to excessive suction on the inner portion of the lower element.

As the stagger is increased to 0.2c, at Mach number of 1.6, the bow shock wave attaches to the two leading edges and the throat area is capable of carrying the mass flow rate and hence the flow choking is completely alleviated. This results in a low drag coefficient of 0.0187 at a free stream Mach number of 1.6. At this configuration, the right running shock wave from the top leading edge intersects the left running shock wave from the lower leading edge well ahead of the point of maximum thickness. At the point of impingement on the low element, a near normal shock wave is formed which strikes the top element aft of the point of maximum thickness. This result in high pressure on the first half the lower element and on the second half of the upper element. As the stagger is further increased, from 0.2c to 0.5c at the free stream Mach number of 1.6, the extend of high pressure zone on the lower element increases with the near normal shock wave moving closer and closer to the lower leading edge. This also results in smaller region of low pressure on the rearward half of the top element. At a stagger of 0.5c, the oblique shock from top leading edge does not interact with that from the lower edge and a lift and drag coefficients of 0.0414 and -0.0374 respectively are realized.

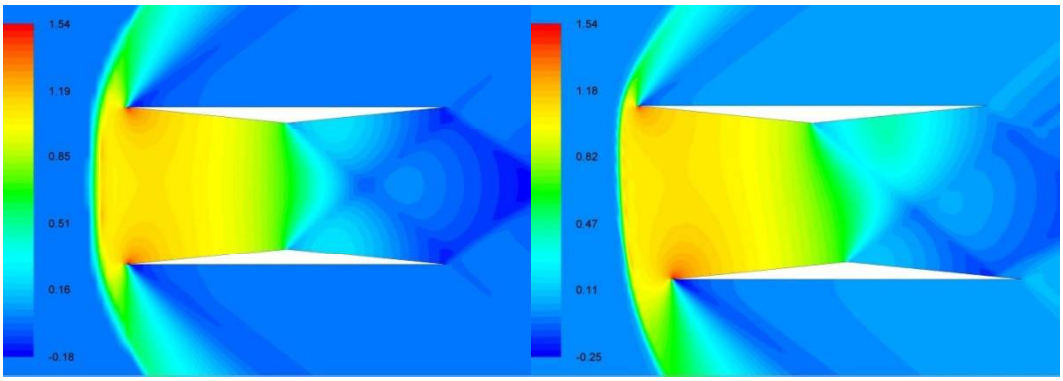

Busemann biplane (C_D = 0.0992, C_L = 0.0000)

Stagger 0.1c (C_D = 0.0949, C_L = 0.1177)

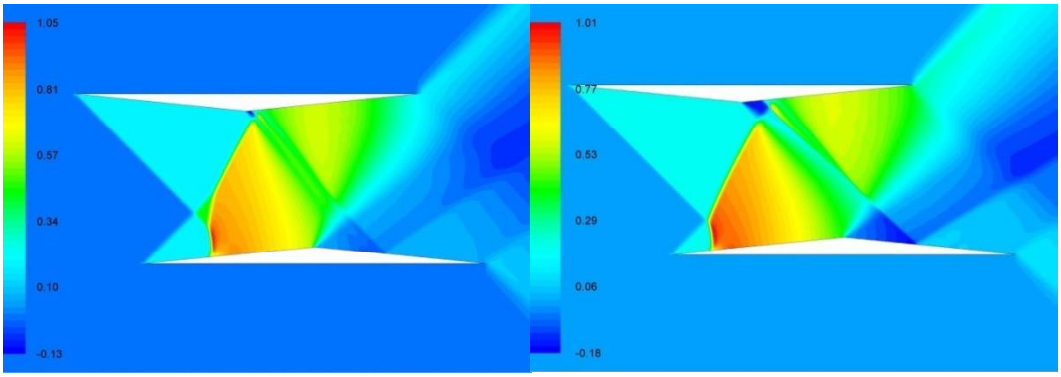

Stagger 0.2c (C_D = 0.0187, C_L = 0.0310)

Stagger 0.3c (C_D = 0.0262, C_L = 0.0085)

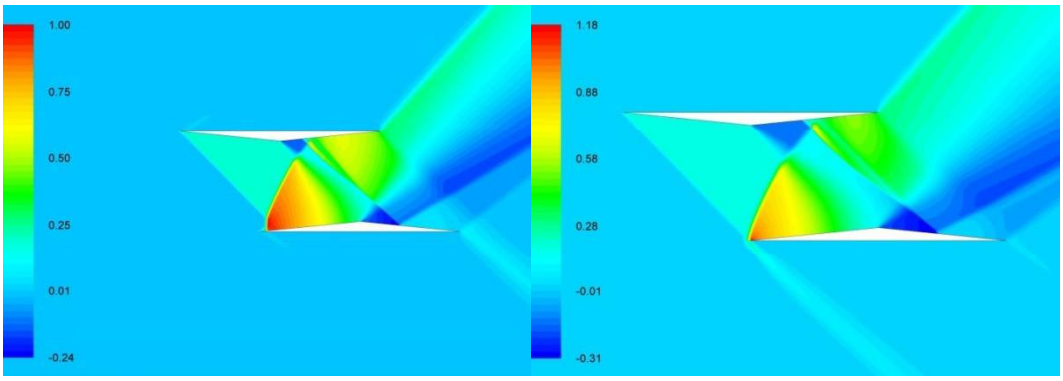

Stagger 0.4c (C_D = 0.0334, C_L = -0.0256)

Stagger 0.5c (C_D = 0.0414, C_L = -0.0374)

Fig. 5.2: Pressure variation with stagger at M_∞ = 1.6 and α =0^o

For lower Mach numbers however, the advantage is lost as can be seen in Fig. 5.3 which shows the contours of pressure coefficients for the different staggered configurations at a free stream Mach number of 1.4.

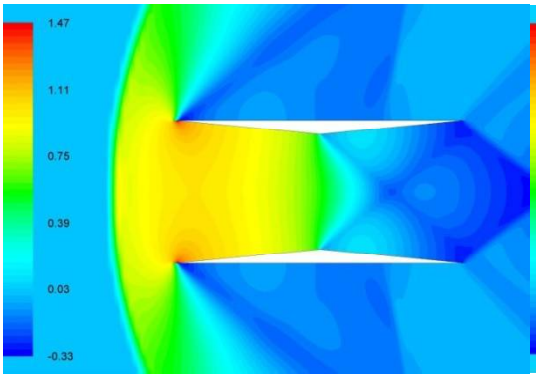

Busemann biplane
($C_D = 0.1044$, $C_L = 0.0000$)

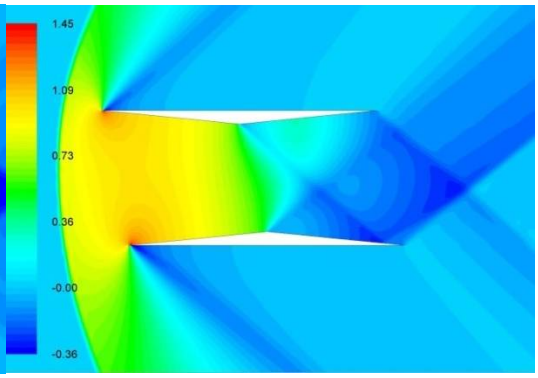

Stagger Upper element 0.1c
($C_D = 0.0996$, $C_L = 0.1275$)

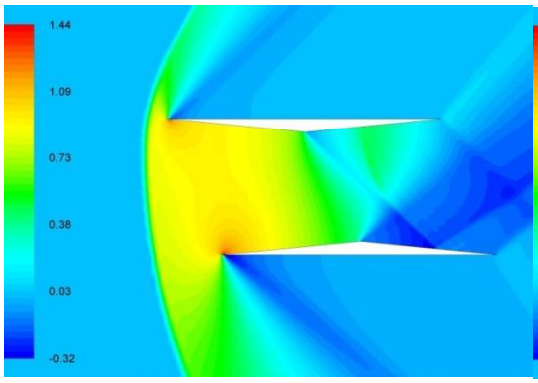

Stagger 0.2c
($C_D c_d = 0.0879$, $C_L = 0.1930$)

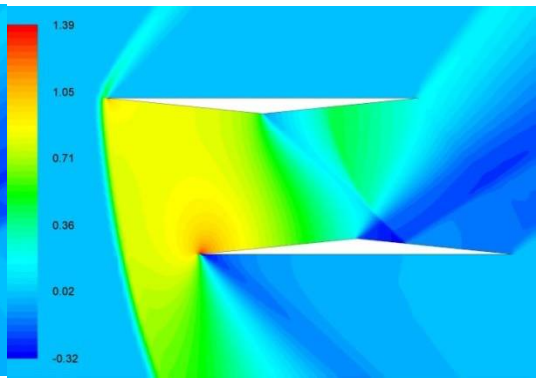

Stagger 0.3c
($C_D = 0.0759$, $C_L = 0.2179$)

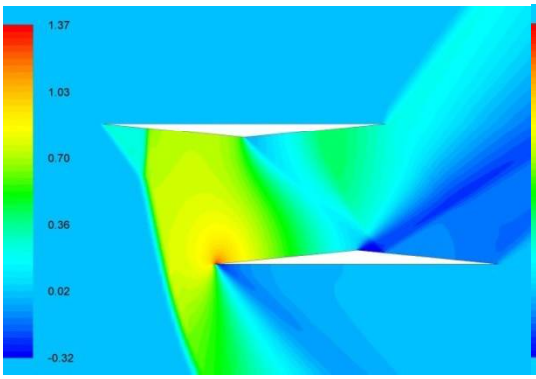

Stagger 0.4c
($C_D = 0.0578$, $C_L = 0.1585$)

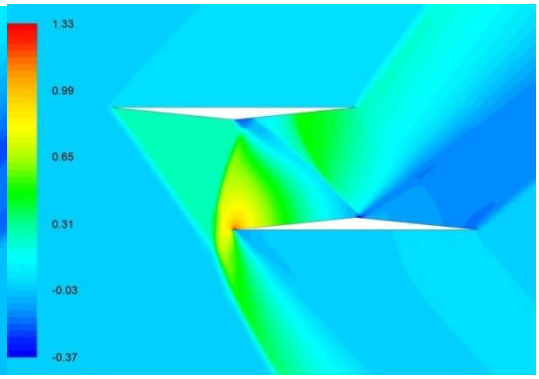

Stagger 0.5c
($C_D = 0.0367$, $C_L = 0.0790$)

Fig. 5.3: Pressure Variation with Stagger distance at $M_\infty = 1.4$ and $\alpha = 0^o$

At this Mach number, the chocking of the flow could not be avoided for any amount of stagger up to 0.5c. The strength of the bow shock and the stagnation pressure is however, significantly lower than that observed for the Busemann biplane band the diamond airfoils and hence a lower drag compared to these airfoils. As the stagger increases, the shock wave attaches to the forward element, however remains detached with that of the rearward element. The rearward element lies completely in the aftershock region of the upwind element. This causes a decrease in the drag of the configuration as the stagger is increased, from 0.1044 to 0.0367 for the stagger distance of 0.5c., due to increased suction on second half of the lower element.

In case of free stream Mach number $M_\infty \geq 1.7$, any stagger results in impinging of the oblique shock from the leading element onto the first half of the rear element resulting in increased pressure on the first half of lower surface and reduced pressure on second half of top element. This causes an increase in the drag of the biplane as compared to that of Busemann configuration. As can be seen in Fig. 5.4, with an increase in the stagger, the regions of high pressure ahead of the point of maximum thickness, increase while the regions of low pressure on the surface aft of the point of maximum thickness for both the elements increase, resulting increased drag.

The variations of drag coefficients with Mach number for different staggered configurations are presented in Fig. 5.5. Figure 5.5 (a) shows the variation from subsonic Mach numbers to design Mach number 1.7 while Fig. 5.5 (b) shows the variation of drag coefficient for Mach numbers higher than 1.7. As can be seen in these figures, a substantial reduction in drag is observed for Mach numbers below the design point through the staggering of airfoils. Although at the design point the Busemann biplane outperforms all the configurations, a consistent reduction of 20- 60% reduction in drag is seen with all staggered configurations throughout the subsonic and transonic range.

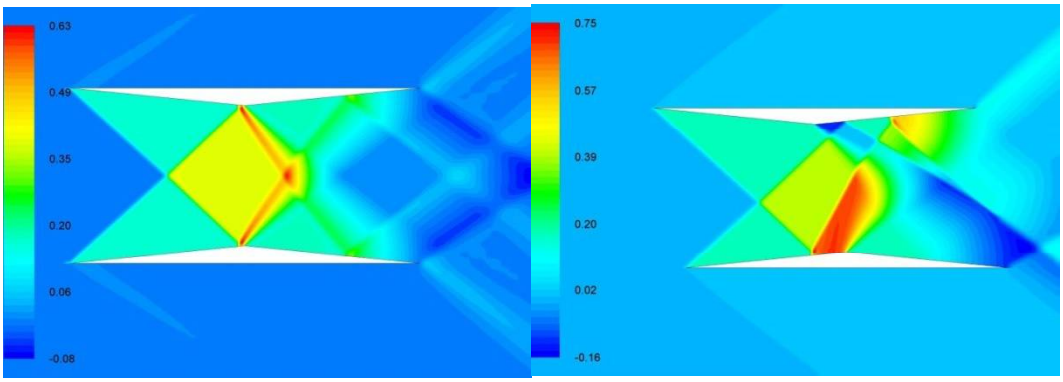

Busemann Biplane (C_D = 0.00989, C_L = 0.0000)

Stagger upper element 0.1c (C_D = 0.0145, C_L c_l = 0.0146)

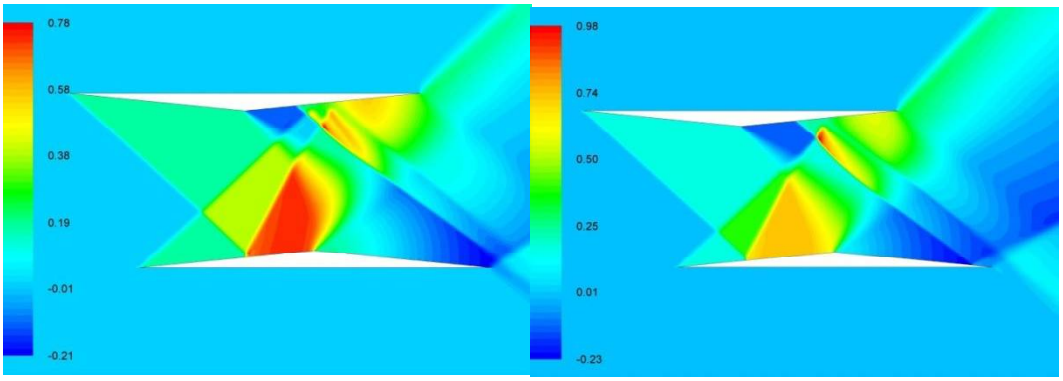

Stagger 0.2c (C_D =0.0224, C_L = 0.0200)

Stagger 0.3c (C_D = 0.0325, C_L = 0.0057)

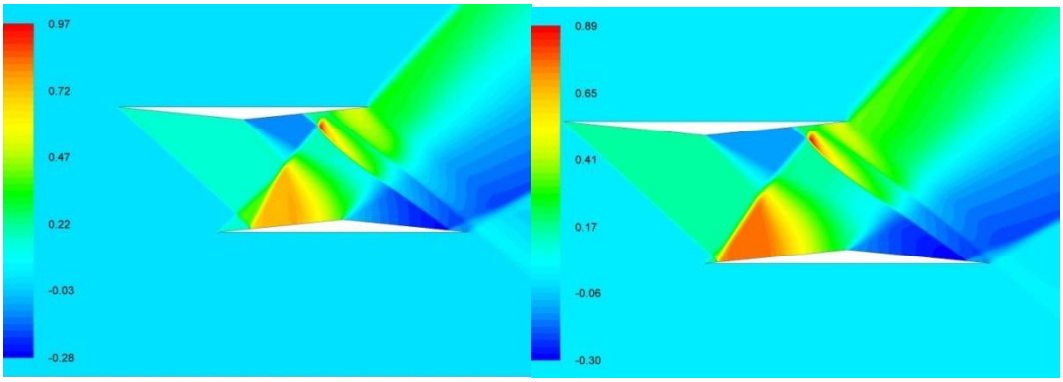

Stagger 0.4c (C_D = 0.0431, C_L = -0.0380)

Stagger 0.5c (C_D = 0.0514, C_L = -0.0620)

Fig. 5.4: Pressure Variation with Stagger at M_∞ = 1.7 and α =0^o

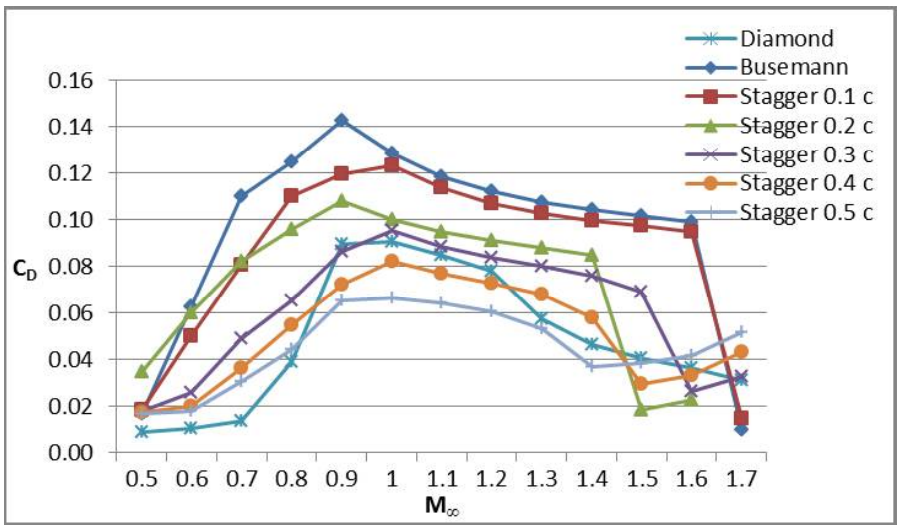

(a)

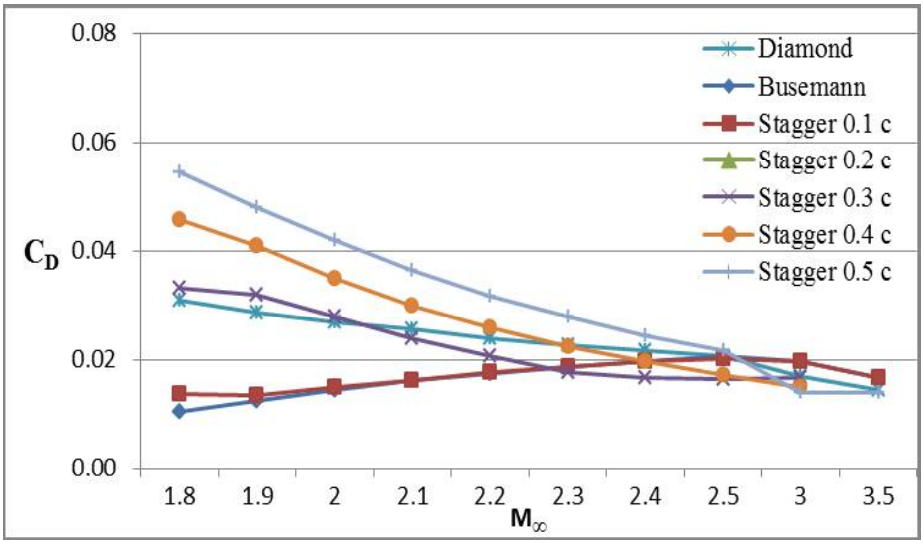

(b)

Fig. 5.5: Drag variation (a) for with M_∞ $0.5 \leq M_\infty \leq 1.7$ and (b) $1.8 \leq M_\infty \leq 3.5$ for different staggered configurations at $\alpha = 0^o$

For Mach numbers above 1.5, an increase in drag coefficient is observed for all configurations, and finally the drag coefficient becomes independent of the stagger for Mach numbers above 2.0 as can be seen in Fig. 5.5 (b). A compromise thus, has to be done with slightly increased drag at design Mach number at the cost of lesser drag from take-off to cruise. The staggering, by increasing the lift coefficient and reducing the drag coefficients, provides an improved aerodynamic

efficiency even at zero degrees angle of attack. The variation of L/D ratio with Mach number at zero degrees angle of attack is shown in Figure 5.6.

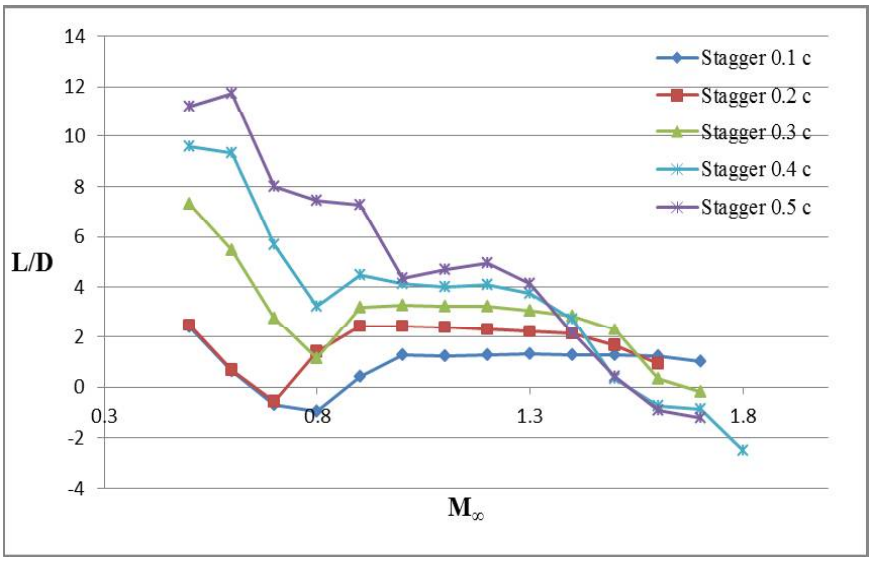

(a) L/D Variation for $0.5 \leq M_\infty \leq 1.7$.

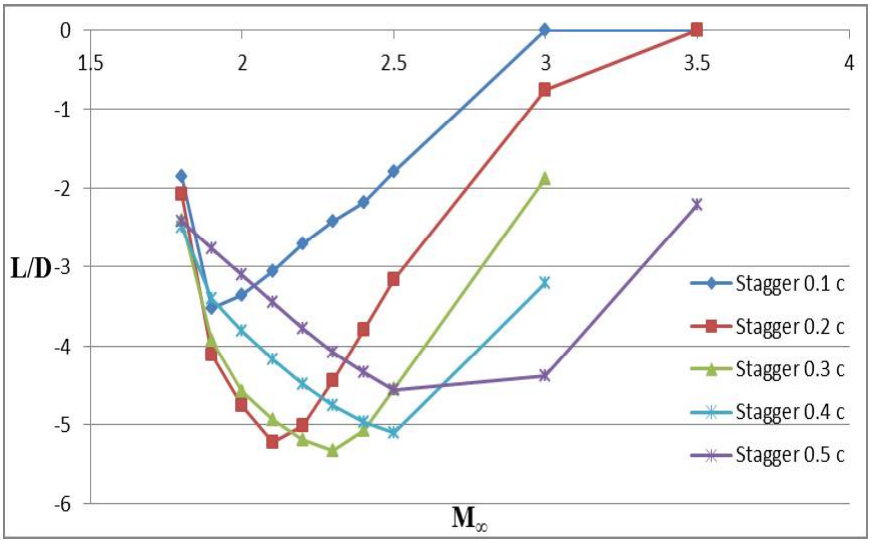

(b) L/D Variation for $1.8 \leq M_\infty \leq 3.5$.

Fig. 5.6: L/D ratio for different Stagger at $\alpha = 0^o$

A high lift to drag ratio observed at subsonic Mach numbers diminishes in value at transonic speeds as can be seen in Fig. 5.6 (a). At supersonic speeds of more

than Mach 1.5, the suction on the surface of upper element, aft of the point of maximum thickness results in negative lift at zero degree angle of attack. This negative lift and associated negative L/D ratio is observed at zero degrees angles of attack even for supersonic speeds up to Mach 3.5 as can be seen in Fig. 5.6 (b).

5.2 Effect of stagger at non-zero angles of attack

For the positive angle of attack α = 1°, and M_∞ = 0.7, the pressure field between the Busemann biplane elements is slightly modified and modified the pressure distribution between the elements. The magnitude of the pressure coefficient increases near the leading edge of the elements, hence this pressure difference increases the lift and drag coefficient for the biplane configuration. In the case of stagger 0.1c, the magnitude of the pressure coefficient is lesser than the Busemann, hence lesser drag and lift coefficients are observed. The magnitude of the drag coefficient decreases from 0.0757 for Busemann to 0.0717 for stagger 0.1c i.e. 5.3% drag reduction is observed and the lift coefficient is decreased from 0.2022 for Busemann to 0.1188 for stagger 0.1c. The pressure variation for Busemann biplane and stagger 0.1c and α = 1° are shown in Figure 5.7.

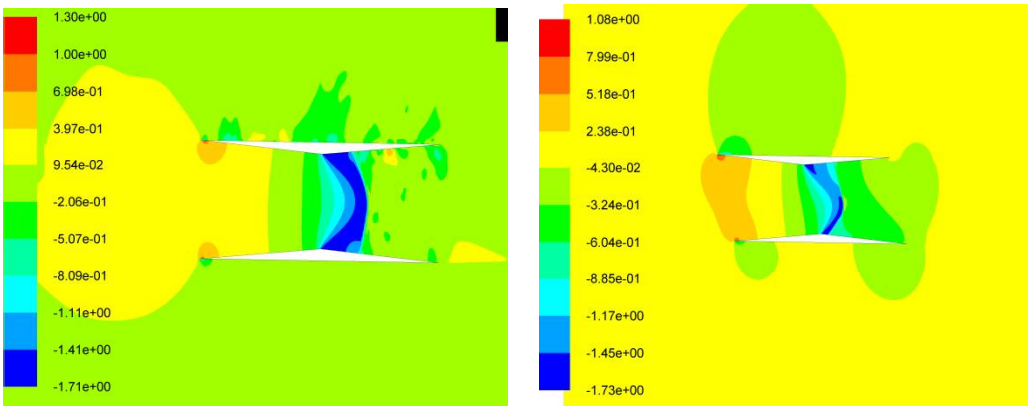

Busemann (C_D = 0.0757, C_L = 0.2022)

Stagger 0.1c (C_D = 0.0717, C_L = 0.1188)

Fig. 5.7 C_p Variation for Stagger 0.1c and 0.2c at M_∞ = 0.7, α = 1°.

With increment in the amount of stagger the magnitude of the stagnation pressure coefficient at the leading edge of the forward element decreases. Besides this, at

the leading edge of the follower element the pressure is significantly lower than the stagnation pressure. This results in a decrease in drag coefficients with stagger as drag coefficient decreases from a value of 0.0717 at stagger 0.1c to 0.040 i.e. around 47% drag decrement is observed at stagger 0.5c. The reduction in magnitude of pressure near the leading edge of the lower element also creates an upward suction, which increases with increasing stagger distance; hence the overall lift coefficient for the combination increases from a value of 0.1188 at stagger of 0.1c to 0.433 at stagger of 0.5c. The variations of pressure field for different staggered biplane configurations are as shown in Figure 5.8.

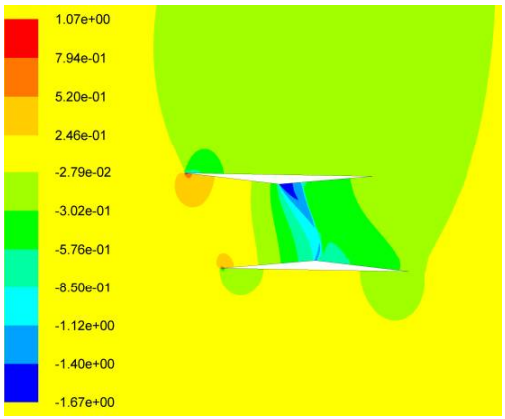

Stagger 0.2c
($C_D = 0.0654$, $C_L = 0.2121$)

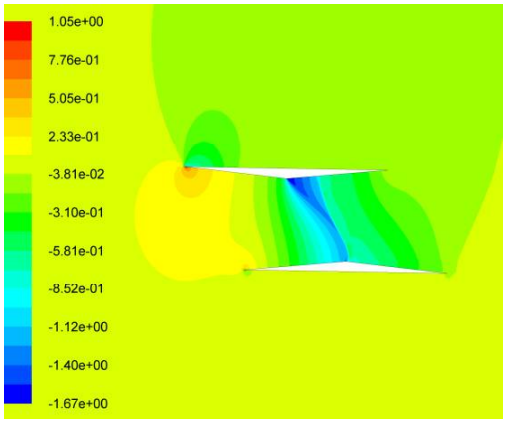

Stagger 0.3c
($C_D = 0.0563$, $C_L = 0.3100$)

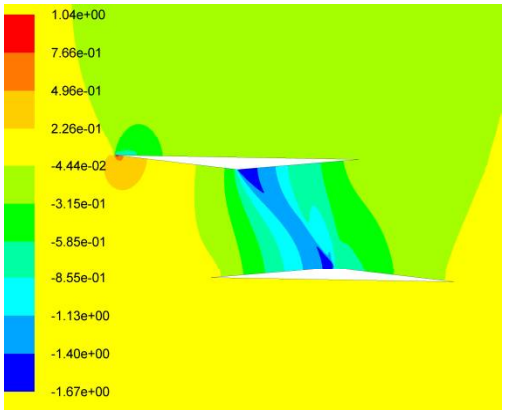

Stagger 0.4c
($C_D = 0.0448$, $C_L = 0.3913$)

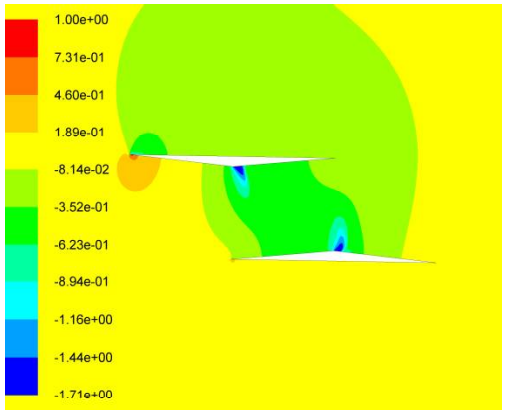

Stagger 0.5c
($C_D = 0.0400$, $C_L = 0.4330$)

Figure 5.8 C_p Variation for different Stagger distance at $M_\infty = 0.7$, $\alpha = 1°$.

For $M_\infty = 0.7$ as the angle of attack is increased to $\alpha = 3°$ at, the magnitude of the pressure on the inner surface of the top element increases while the pressure on the upper surface of the both elements reduces due to the expansion of flow over these surfaces. Bothe the increase in pressure on lower surfaces and reduction in pressure on upper surfaces are emphasized with the increasing stagger distance. For this combination the overall drag coefficient decreases from 0.1402 for the Busemann to 0.0776 at stagger 0.5c i.e. around 45% of reduction in drag coefficient is observed. The magnitude of lift coefficient is also observed to increase from 0.5531 for the Busemann to 0.8343 at stagger 0.5c. The pressure variations around staggered Busemann biplanes at $\alpha = 3°$ and freestream Mach number of 0.7 is shown Fig. 5.9.

As the freestream Mach number is increased to a supersonic value of $M_\infty = 1.7$ for positive angles of attack $\alpha = 1°$, the pressure difference between the top and bottom surfaces of the upper element is further increased due to the expansion waves induced over the top surface and an increase in shock wave strength on the lower side due to increase in deflection angle. For the lower element the strength of the shock between the elements decreases with an increase in angle of attack. As the shock angle for the left running shock wave decreases, the overall pressure on the top surface of the lower element decreases, hence a net lift coefficient of 0.0593 and the drag coefficient of 0.110 are observed for the Busemann biplane. For a stagger of 0.1c, the pressure difference on the upper forward element is enhanced which increases the overall lift and drag coefficient to 0.0850 and 0.172 respectively. The pressure field around the biplane configurations at Mach number of 1.7 and $\alpha = 1°$ is shown in Figure 5.10.

With an increment in the stagger at $\alpha = 1°$ and $M_\infty = 1.7$, the shock strength for the top surface is decreased while the region of high pressure on the inner surface of lower element increases. This results in a decrease lift while an increase in drag is observed as the high pressure on the bottom surface is ahead of the mid-section

which contributes to positive drag and negative lift. The variation of pressure for various staggered configuration at $\alpha = 1°$ and $M_\infty = 1.7$ is shown in Fig. 5.11.

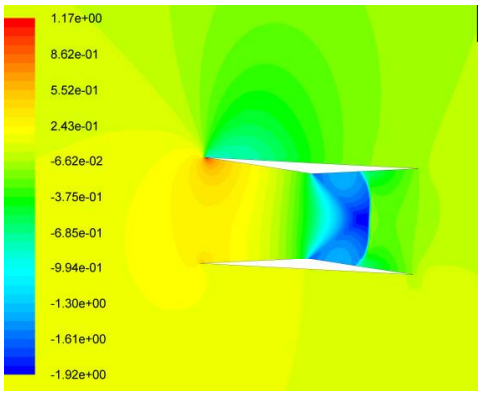

Busemann
($C_D = 0.1402$, $C_L = 0.5531$)

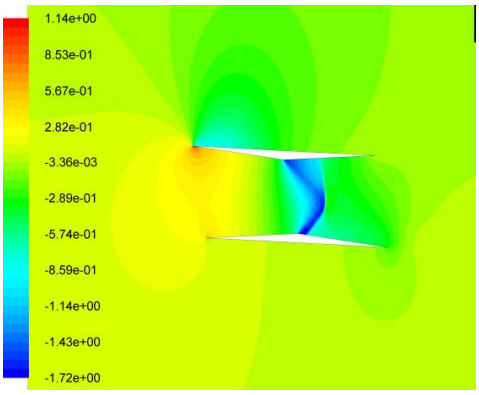

Stagger 0.1c
($C_D = 0.1080$, $C_L = 0.4576$)

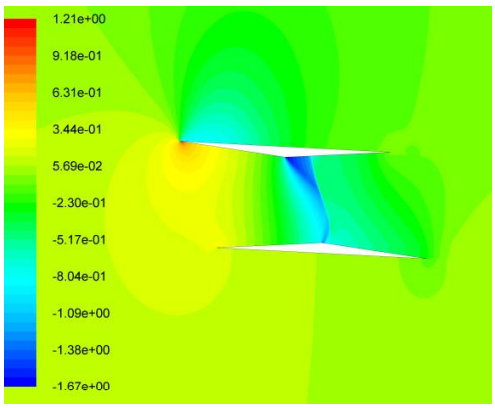

Stagger 0.2c
($C_D = 0.0941$, $C_L = 0.5830$)

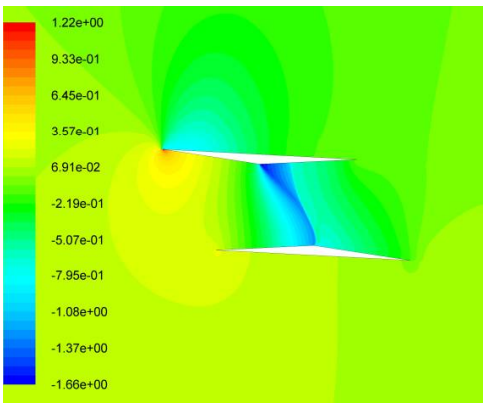

Stagger 0.3c
($C_D = 0.0890$, $C_L = 0.6858$)

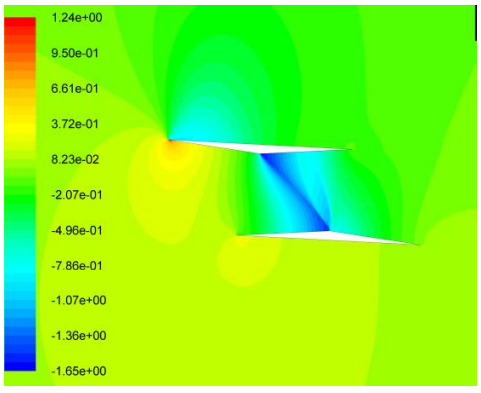

Stagger 0.4c
($C_D = 0.0816$, $C_L = 0.7865$)

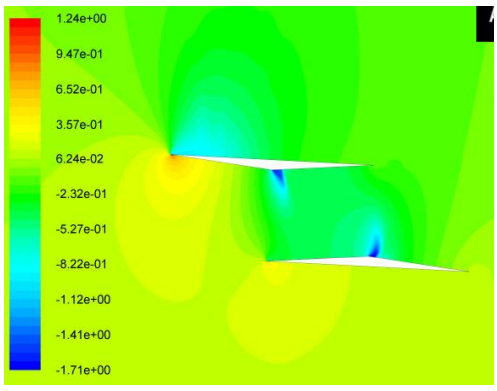

Stagger 0.5c
($C_D = 0.0776$, $C_L = 0.8343$)

Fig. 5.9 C_p Variation for different Stagger distance at $M_\infty = 0.7$, $\alpha = 3°$.

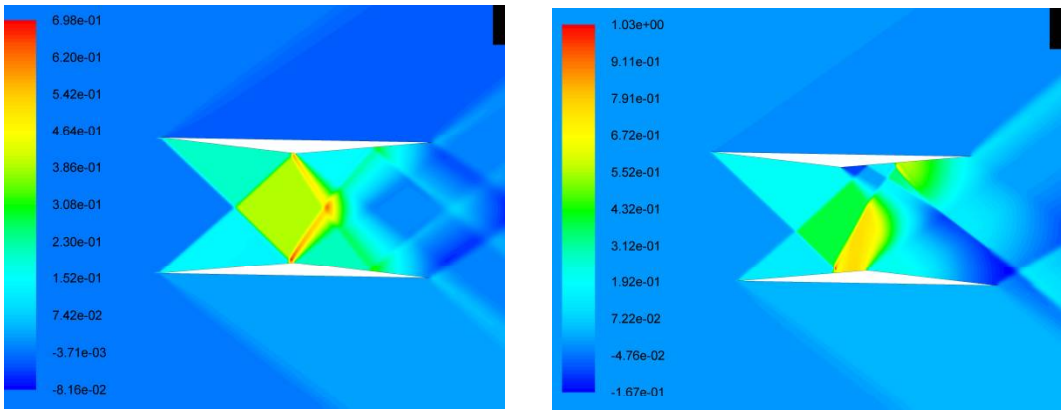

Busemann ($C_D = 0.0110.$, $C_L = 0.0593$)

Stagger 0.1c ($C_D = 0.0172$, $C_L = 0.0850$)

Fig. 5.10 C_p Variation for Busemann and Stagger distance 0.1c at M_∞=1.7, $\alpha = 1°$

As can be seen in Fig. 5.11, with an increase in stagger the interactions between the right running and the left running shock waves between the elements are such that, the region of high pressure on lower element ahead of mid-section increases with stagger. It can also be observed in Fig. 5.11 that the stagger also increases the region of low pressure aft of the mid-section both on lower and upper surfaces. Thus results in substantial increase in drag of the biplane at the design Mach number of 1.7. At an angle of attack of 1°, the drag coefficient increases from 0.0172 at stager of 0.1c to 0.05 at a stager of 0.5c.

For even higher values of angle of attack $\alpha = 3°$, $M_\infty = 1.7$, the drag coefficient is further increased due to the strengthening the expansion waves on the top of the upper element and the shock waves between the elements. Owing to the increased suction on upper element the value of lift coefficient increases from 0.18 for the Busemann to 0.2465 at stagger 0.2c. But with increasing stagger, the extent of high pressure region aft of the near normal shock formed on the top surface of the lower element increases. This results in a reduction in lift with increasing stagger at $M_\infty = 1.7$ and $\alpha = 3°$ wherein the lift coefficient reduces to 0.1275 for a stagger of 0.5c. The increased pressure on the lower element also results in increased drag

which goes up to 0.05 for a stagger of 0.5c. The shock-shock interactions and the regions of high pressure on the top surface of the lower element can be clearly seen in Fig. 5.12 which shows the contours of C_p variation at $M_\infty = 1.7$ and $\alpha = 3°$ for different staggered configuration. Figs. 5.9, 5.10 and 5.12 show the shock-shock interactions and shock-expansion wave interactions through the contours of pressures, for selected cases mentioned above and a comprehensive pressure contours for various Mach numbers and angles of attacks are compiled and presented in Appendix A.

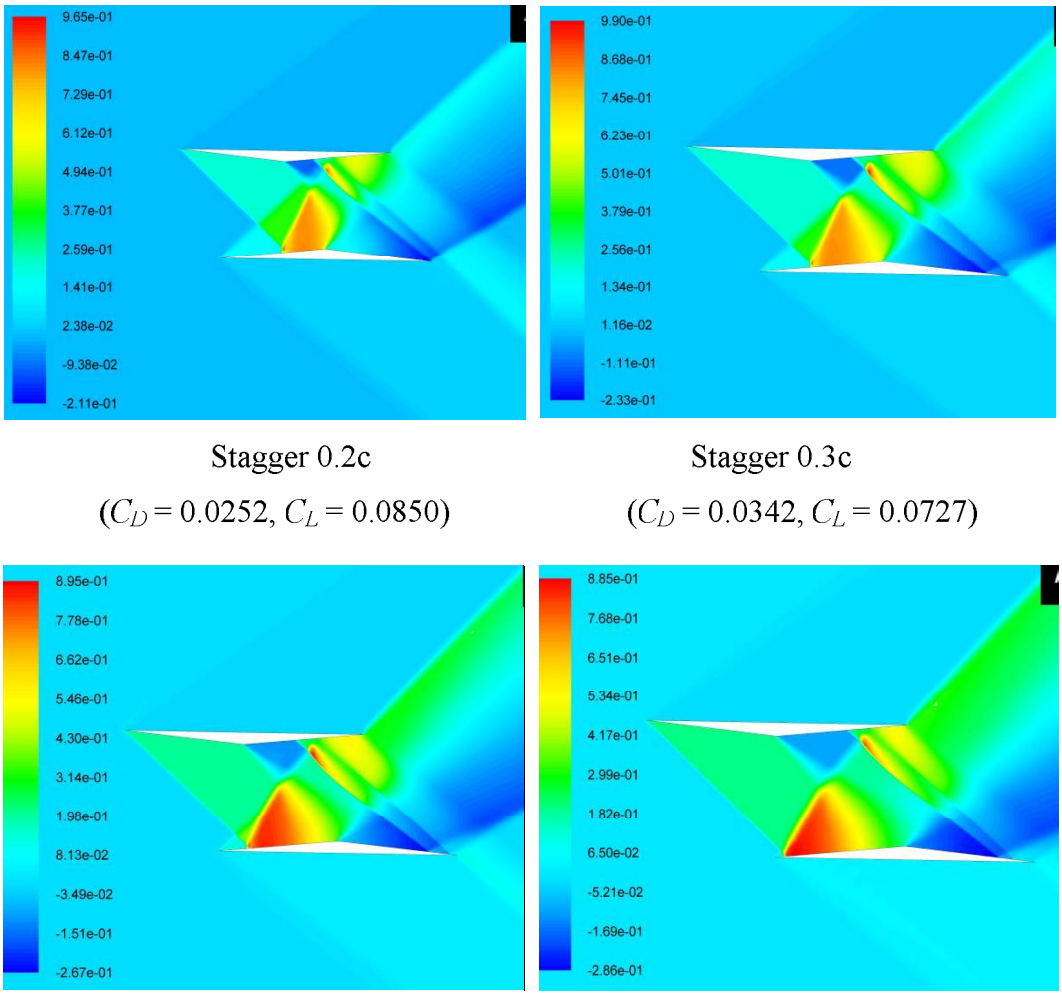

Stagger 0.2c ($C_D = 0.0252$, $C_L = 0.0850$)

Stagger 0.3c ($C_D = 0.0342$, $C_L = 0.0727$)

Stagger 0.4c ($C_D = 0.0427$, $C_L = 0.0324$)

Stagger 0.5c ($C_D = 0.0500$, $C_L = 0.001$)

Fig. 5.11 C_p Variation for different Stagger distances at $M_\infty = 1.7$ and $\alpha = 1°$.

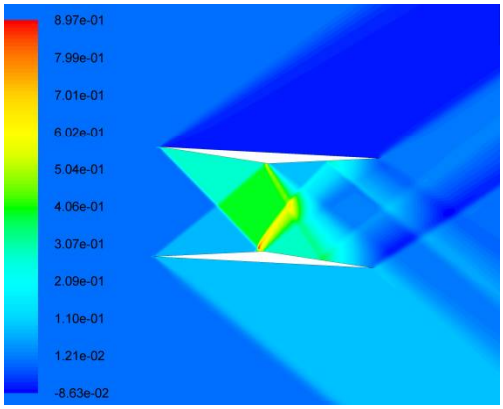

Busemann
($C_D = 0.0200$, $C_L = 0.1800$)

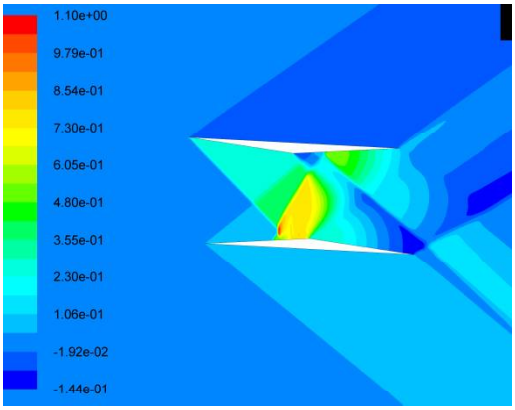

Stagger 0.1c
($C_D = 0.0284$, $C_L = 0.2232$)

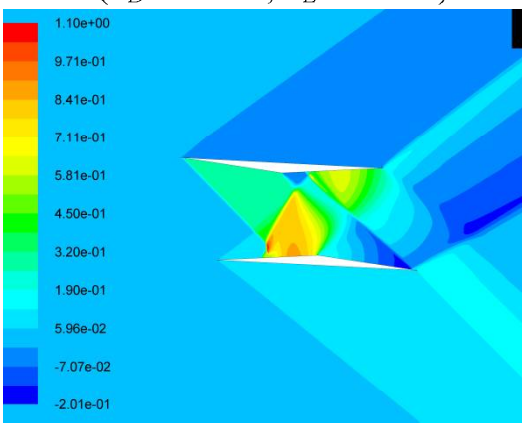

Stagger 0.2c
($C_D = 0.0380$, $C_L = 0.2465$)

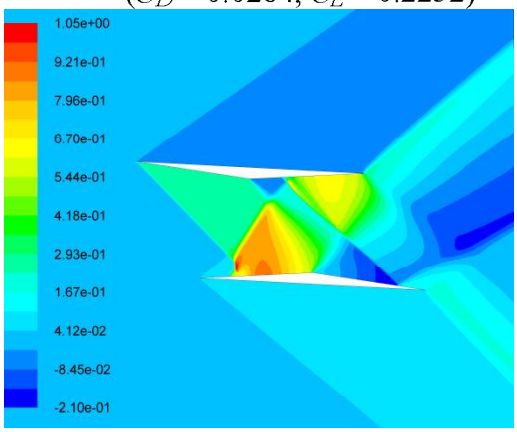

Stagger 0.3c
($C_D = 0.0424$, $C_L = 0.2095$)

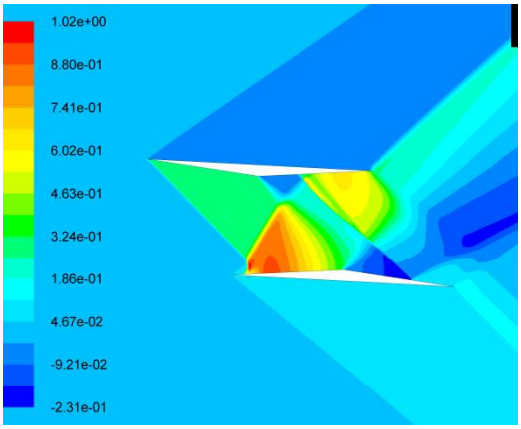

Stagger 0.4c
($C_D = 0.0465$, $C_L = 0.1605$)

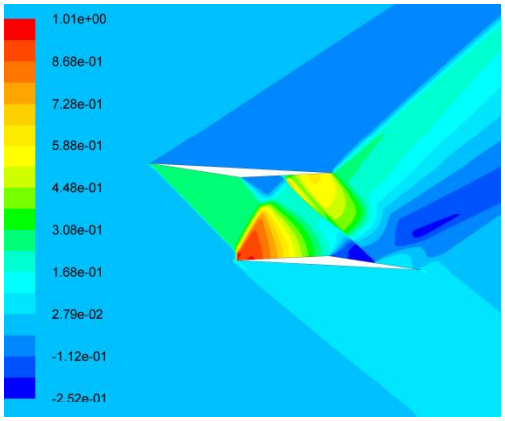

Stagger 0.5c
($C_D = 0.0500$, $C_L = 0.1275$)

Fig. 5.12 C_p Variation for different Stagger distances at $M_\infty = 1.7$ and $\alpha = 3°$.

The changing shock-shock interactions between the staggered elements result in significant changes in the drag of the biplane with changing stagger at all Mach numbers as can be seen in Fig. 5.13. As can be seen in Fig. 5.13 a, b and c, the magnitude of the drag coefficient increases with the angle of attack due to increasing shock strength of the right running shock wave from the leading upper element. At all angles of attack, however, the drag is favourably reduced for the staggered configurations for Mach numbers less than the design Mach number of 1.7. For Mach numbers higher than 1.7, the staggered biplanes suffer from increased drag coefficients as can be seen in Fig. 5.13. At an angle of attack of 1°, the reduction in drag observed with staggered configuration is significant at the sub-design Mach numbers as can be seen in fig. 5.13 a. The reductions in drag obtained for these Mach numbers are in the range of 40%-60 % for various amount of stagger. As the angle of attack is increased, the amount of reduction in drag observed for staggered configurations diminishes as can be seen in fig. 5.13 a, b and c. The drag coefficients of the staggered configurations are however, unaffected by the increase in angles of attack at Mach numbers higher than 1.7.

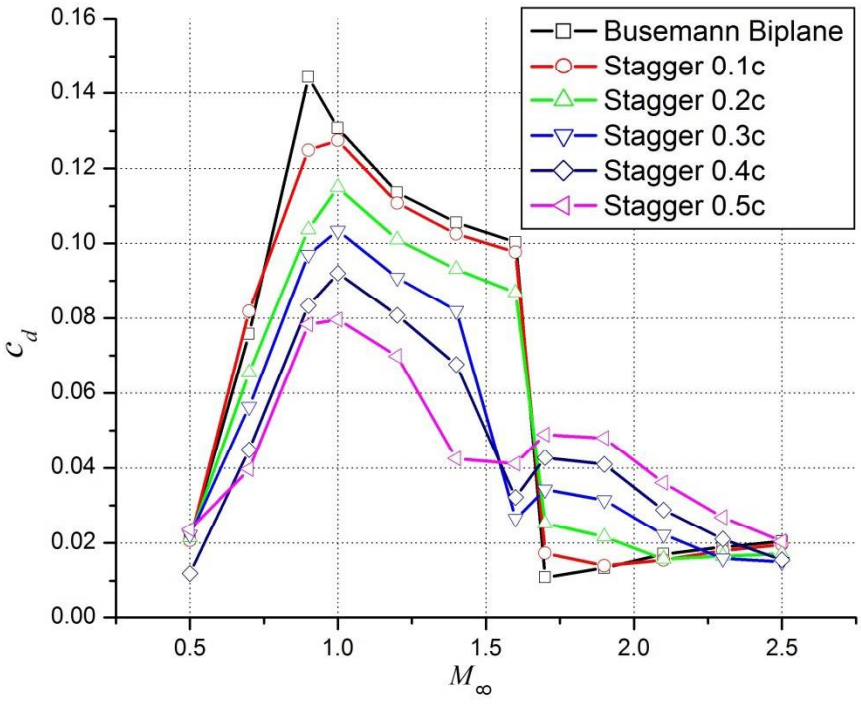

(a) Drag Variation at $\alpha = 1°$.

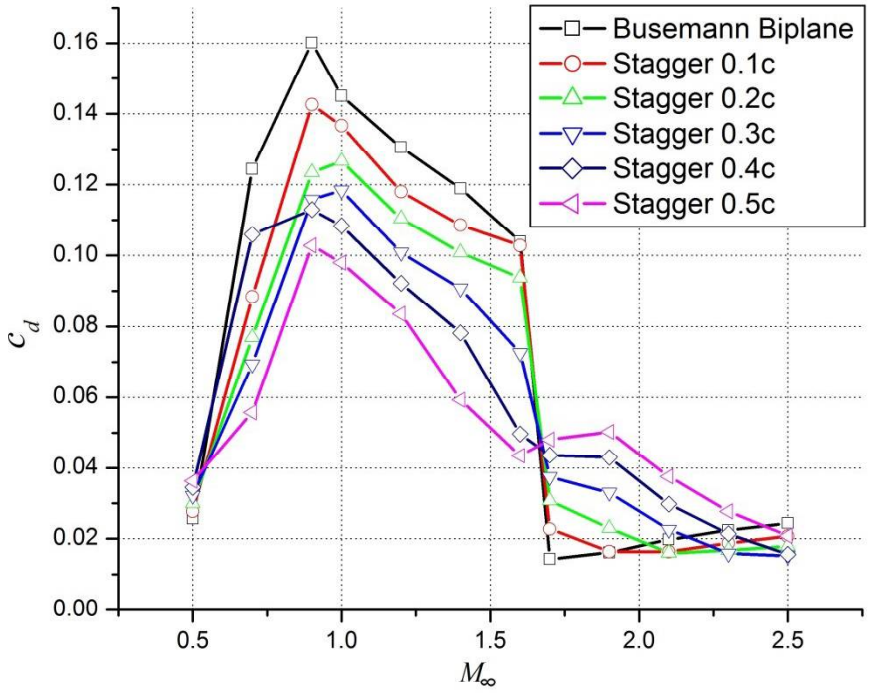

(b) Drag Variation at $\alpha = 2°$.

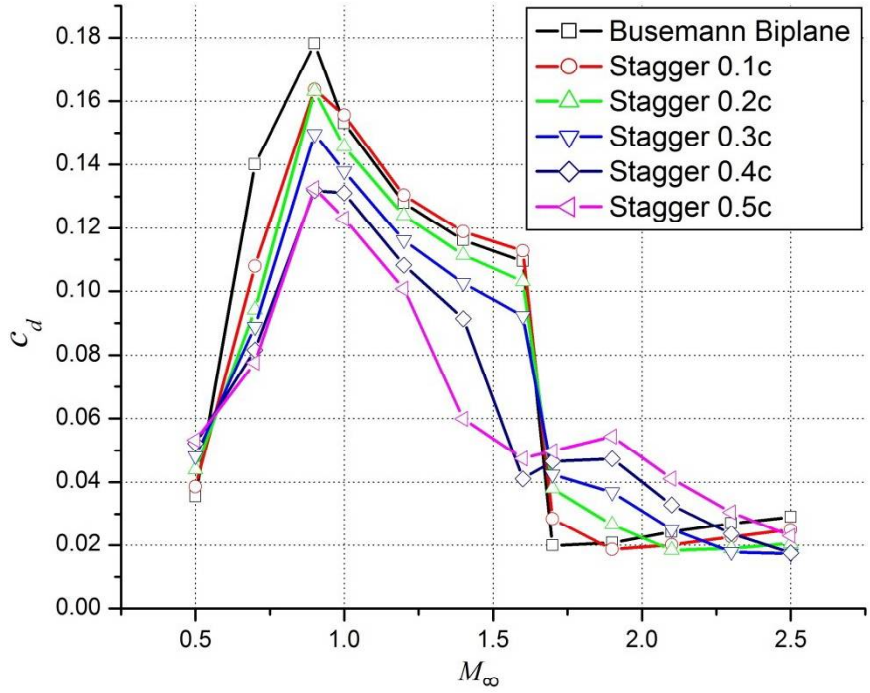

(c) Drag Variation at $\alpha = 3°$

Fig. 5.13: C_D Variation at different angle of attack with M_∞

At positive angles of attack both the top and bottom elements contributes positively to the biplane lift. The introduction of stagger improves the aerodynamic efficiency of the biplane at all Mach numbers less than the design Mach number for Busemann biplane as can be seen in Fig. 5.14. At an angle of attack of 1^{o}, the flowfield is only slightly modified from that of zero degrees angle of attack and the configuration is associated with negative lift production at Mach numbers higher than 1.7 as is clear from the negative *L/D* ratios at these Mach numbers.

Due to an increase in lift and decrease in drag coefficients for the staggered configurations at $M_{\infty} \leq 1.7$, the *L/D* ratio for these configurations are higher than those of the Busemann biplane configuration as can be seen in Fig. 5.14. At α = 1°, and M_{∞} = 0.5, the staggered biplane configuration with 0.5c stagger gives L/D ratio that is more than twice for that for a Busemann biplane. As the Mach number increases from low subsonic to transonic and supersonic Mach numbers, the increase in *L/D* ratio diminishes for all amount of stagger as can be seen in Figs. 5.14. Nevertheless, all staggered configurations except the one with a stagger of 0.1c provides an improvement in *L/D* ratio at sub design Mach numbers and α = 1°. For the design Mach number of 1.7 and at $M_{\infty} \geq 1.7$, the original Busemann biplane configuration offers the best *L/D* ratio at α = 1°. In fact, due to the negative lift provided by the staggered configurations at Mach numbers higher than 1.7, negative values of *L/D* ratios can be observed the these Mach numbers as can also be seen in Fig. 5.14. This drop in the *L/D* ratio can be observed to increase with an increase in the amount of stagger.

At higher angles of attack there is further increment in *L/D* values at lower freestream Mach numbers and a subsequent reduction for the higher freestream Mach numbers. At angles of attack at $\alpha = 2^{o}$ and $\alpha = 3^{o}$, the suction on external surface of upper element and high pressure on external surface of bottom element dominates the lift produced by the internal surfaces. So the negative lift and thus the negative *L/D* ratios seen at large Mach numbers disappears for these angles of attack as can be seen in Figs. 5.15 and 5.16. For all these cases, it has been found

that the *L/D* ratio is decreases with an increase in the freestream Mach number and found to reduce with an increase in stagger. The maximum *L/D* ratio among the cases investigated have been observed to be 15.73 for staggered configuration of 0.5c at $\alpha = 3^{o}$.

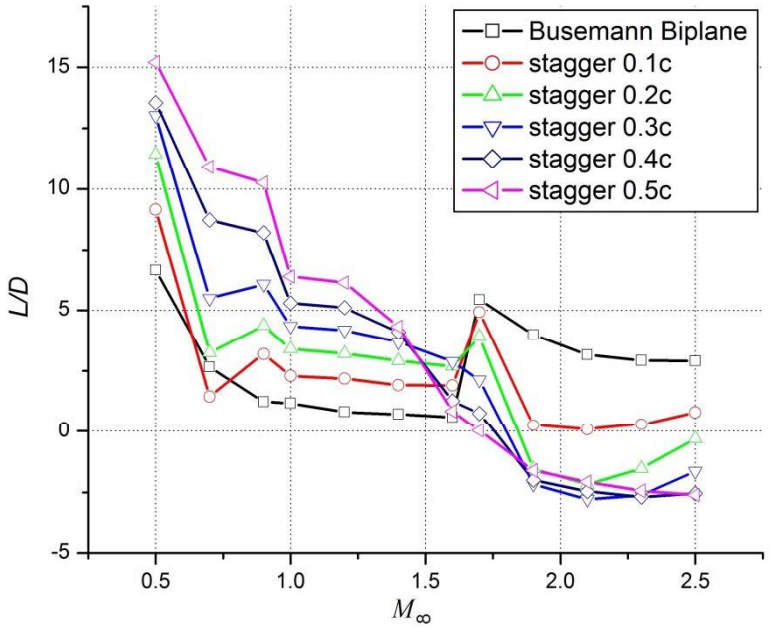

Fig. 5.14: L/D ratio of different stagger configuration at α= 1^{o}

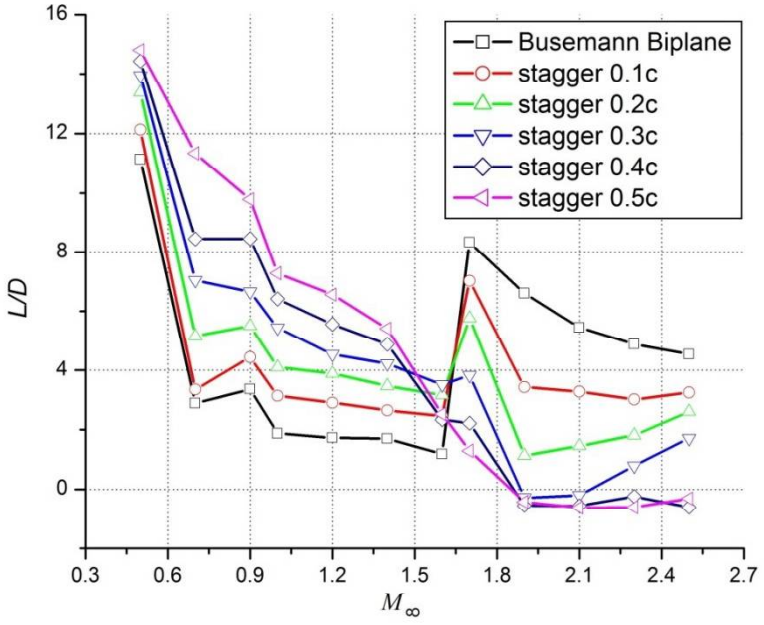

Fig. 5.15: *L/D* ratio of different stagger configuration at $\alpha = 2^{o}$

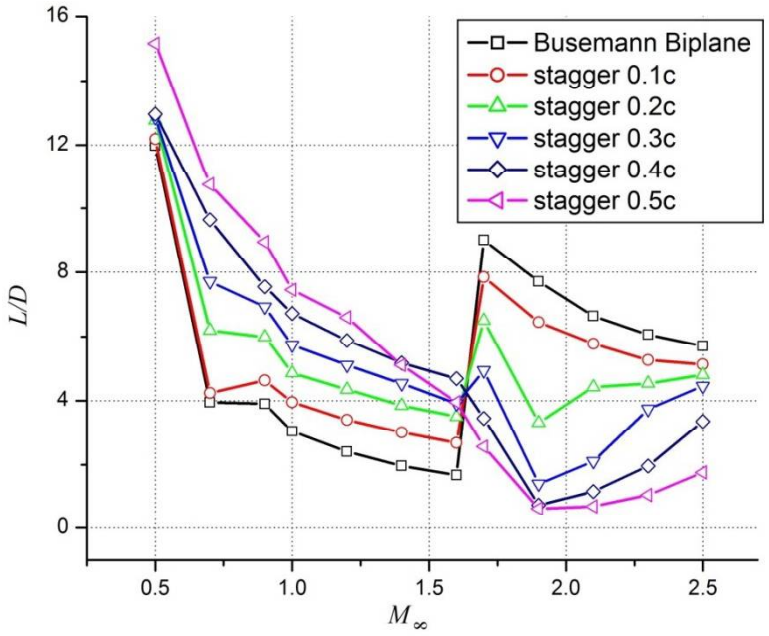

Fig. 5.16: L/D ratio of different staggered configuration at $\alpha = 3^{o}$

Thus very favorable L/D ratios can be realized at subsonic speeds for Busemann biplanes by staggering the configuration. For all the Mach numbers, the L/D ratio increase almost linearly with an increase in angle of attack for the range investigated as can be seen in Figs. 5.17 and 5.18. Although in terms of the aerodynamic efficiency, the original Busemann biplane outperforms other configurations at high Mach numbers, the staggering certainly helps at Mach numbers below the design Mach number of 1.7. For a very large stagger of 0.5c however, the increase in aerodynamic efficiency with angle of attack ceases especially at low Mach numbers. In fact, for subsonic Mach numbers a decrease in aerodynamic efficiency can be observed as the angle of attack of the configuration is increased. At supersonic Mach numbers below the design Mach number of 1.7, the reduction in aerodynamic efficiency for Busemann biplane is recovered slightly with the staggering of the biplanes. These improvements seen for sub-design Mach numbers for staggered configurations are primarily due reduction in wave drag for these configurations. As can be seen in Fig. 5.18, for the design and higher supersonic Mach numbers the original Busemann biplane configuration outperforms the staggered configurations.

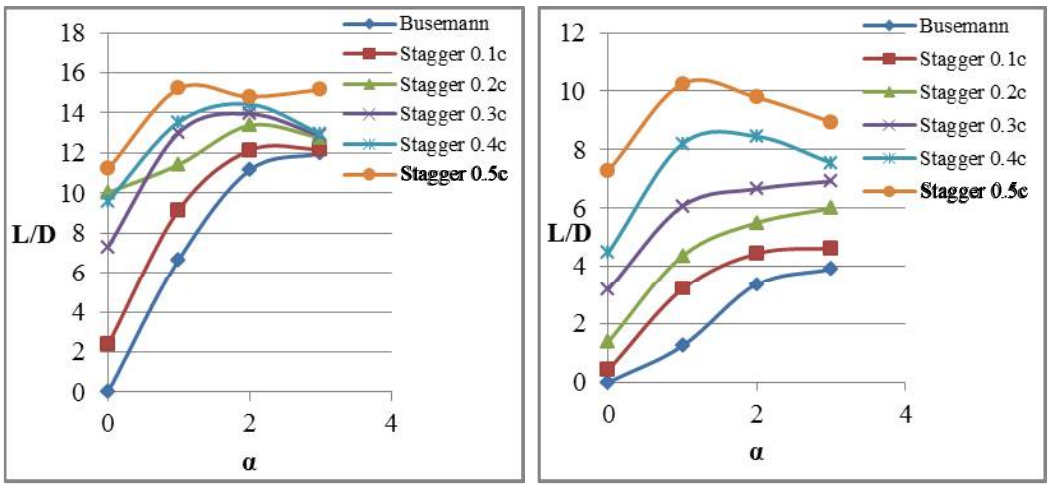

(a) $M_\infty = 0.5$. (b) $M_\infty = 0.9$.

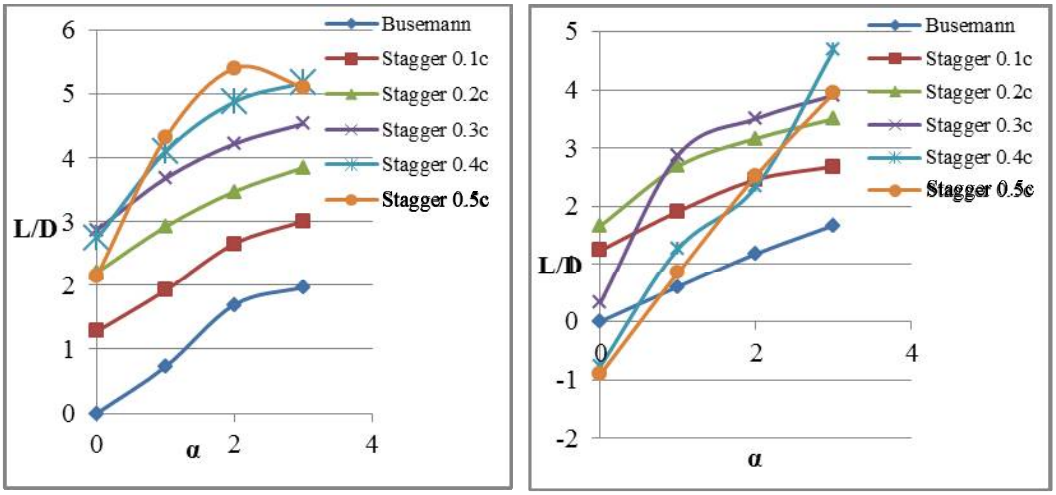

(c) $M_\infty = 1.4$ (d) $M_\infty = 1.6$

Fig. 5.17 L/D Variation with angle of attack at $0.5 \leq M_\infty \leq 1.7$.

In conclusion, it can be said that the subsonic and low supersonic aerodynamic characteristics of the Busemann biplane can be greatly improved by the staggering of biplanes. The Busemann biplane which shows extremely reduced drag at the design Mach number of 1.7, exhibits undesired aerodynamic characteristics at off design Mach numbers, especially below 1.7.

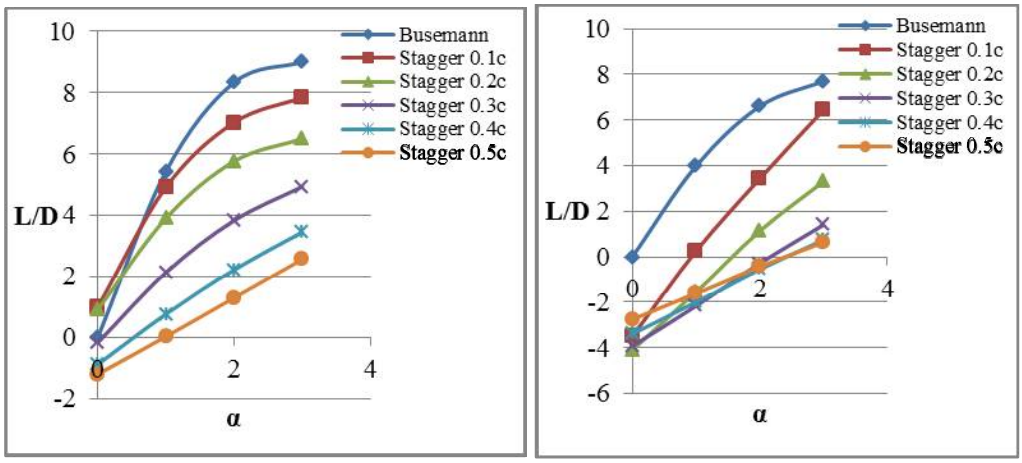

(a) $M_\infty = 1.7$ (b) $M_\infty = 1.9$

Fig. 5.18 L/D Variation with angle of attack at $M_\infty = 1.7$ & 1.9.

The chocking phenomena seen in Busemann biplane for a Mach number of 1.6, is alleviated by a stagger of 02.c or more. At lower supersonic Mach numbers, although the choking is not completely eliminated by staggering, the shock wave attached to the leading element is weaker than a bow shock and thus a reduced drag is observed at all Mach numbers. The advantage of using stagger is highly justifiable in the subsonic range where not only the drag is reduced significantly, but a substantial increase in lift is observed. The staggered configuration have shown a consistent list due to lower element suction even at 0^o angle of attack giving L/D ratios of up to 12. The reduction in drag increases with increase in stagger, however the increase in lift diminishes with increasing stagger. The L/D ratio or the aerodynamic efficiency however, in subsonic and transonic range is significantly higher than those for Busemann biplane at all angles of attack. For staggered configurations at Mach numbers between 0.5 And 1.6, an increment of 175% to 67% in L/D ratios is observed at $\alpha = 3^o$. At Mach 1.7 and higher, the Busemann outperforms all staggered configurations because of small wave drag of the Busemann biplane and negative lift shown by staggered configurations, especially at $\alpha = 0^o$.

5.3 Effect of Leading and Trailing Edge radii on Busemann

Most of the research done on supersonic biplanes and the shock wave cancellation effects assumes that the biplane elements have sharp leading and trailing edges which results in attached oblique shock waves at the leading edges. This also means a perfect shock cancellation and hence ideal scenarios of zero pressure drag. From structural point of view and also from the point of manufacturing difficulties, perfectly sharp edges are impractical. In supersonic flow, the shock waves are generated at the sharp edge, hence the pressure at the sharp edge becomes very large and generate large amount of force at the sharp edge. The edge of the element must be strong enough to resist the pressure increment by the shock waves; therefore it is necessary to use the rounded leading edge. Hence this section provides with the performance of the original and the staggered biplanes with rounded leading and trailing edges.

The numerical simulations are done for different leading edge and trailing edge radius (1mm, 2mm, 3mm and 5mm) for the Busemann biplane as well as for the different stagger configuration discussed in section 4.1(check this numbers), and the typical biplane geometry with rounded leading edge is as shown in Fig. 5.19. The rounding off of the sharp leading and trailing edges results in slightly shorter chord length for these elements. The reduction in length is however negligible and do not produce any significant loss of accuracy for computation of aerodynamic coefficients.

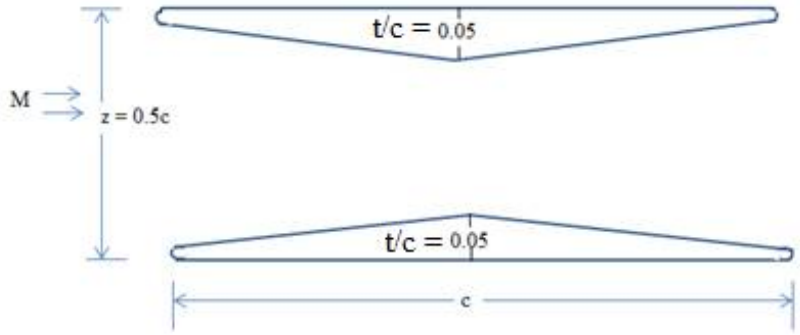

Fig. 5.19: The Busemann biplane with rounded leading and trailing edges

The thickness to chord ratio for each element is t/c = 0.05 and distance between the elements is set to 0.5, so that the results obtained from the current analysis easily comparable with the standard Diamond airfoil and Busemann biplane configuration. The grids topology and the number of elements used along with the solution strategy is also similar to that used for earlier cases so as to maintain the same levels of accuracy in the results. The mesh element with the leading and trailing edge radius is as shown in Fig. 5.22.

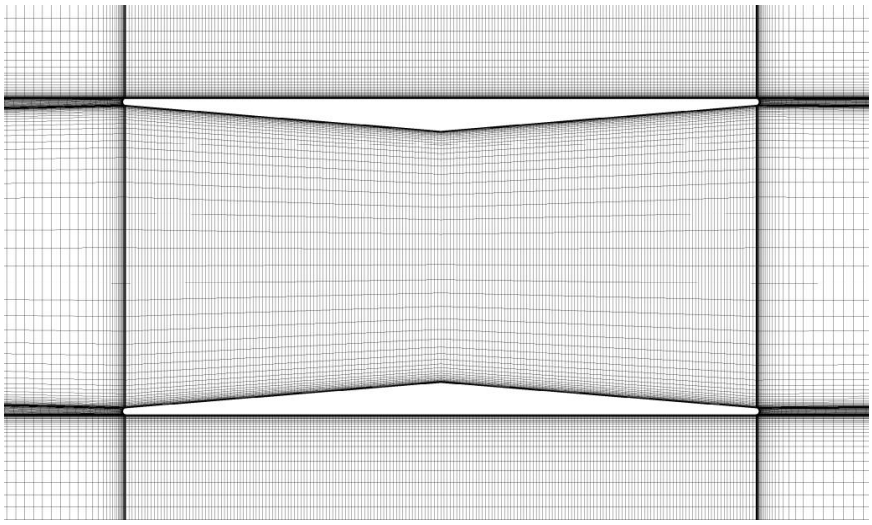

(a) Busemann Biplane

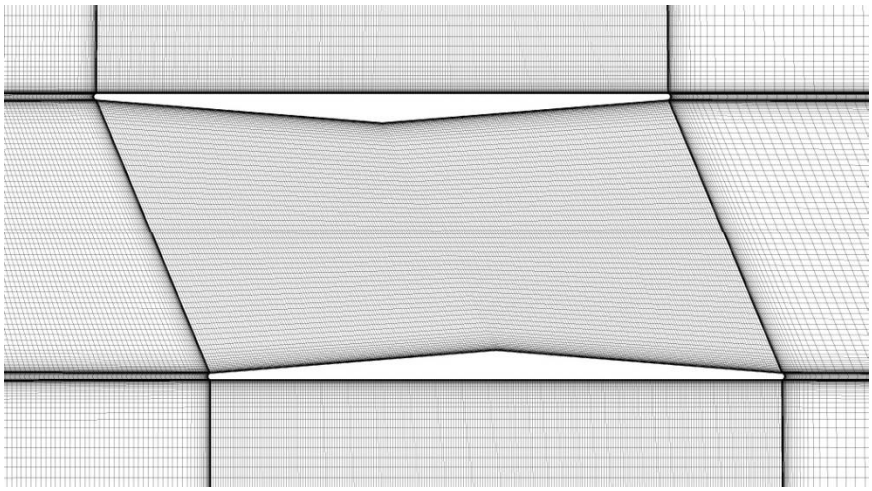

(b) Staggered biplane configuration

Fig. 5.20: Multi-block Grid around biplanes with rounded leading and trailing edges

For a subsonic freestream flow over Busemann biplanes with sharp leading edge, there is no real stagnation point and flow passes over the outer surfaces without much of acceleration or decelerations. On the inner surfaces the flow is slightly decelerated near the leading edges with subsequent rise in pressure. Owing to a convergent section, the subsonic flow accelerates thereafter till the mid-section with to low pressure. For a freestream Mach number of 0.6 and higher and the flow accelerate to supersonic Mach numbers in the divergent section with consequent drop in the static pressure. The lower pressure in the region aft of the mid-section as compared to that ahead of it results in the observed drag. For the Busemann biplane with rounded leading edges, there is a finite region of stagnation at the leading edge. The rounded leading edges make the flow to accelerate on both the outer and inner surfaces smoothly to reach low pressures and higher Mach numbers. This results in subsequent reduction in drag with increasing radius of leading and trailing edges. Thus for the rounded leading edges the acceleration of the flow after the mid-section is significantly more than that of sharp leading edge case. This results in a reduction drag for the Busemann biplane with the use of rounded leading and trailing edges due to the fact that the maximum pressure is concentrated to a small region and a highly reduced pressure is observed over a larger area near the leading edge. A typical variation of pressure coefficient around sharp edge and the rounded leading edge of the Busemann biplane with 1 mm radius at $M_\infty = 0.6$ is shown in Fig. 5.21. The drag coefficient for the Busemann biplane decreases from 0.0605 with sharp edge to 0.0618 for 1 mm leading edge radius at zero degree angle of attack. As can be seen in Fig. 5.22, with further increment in the leading edge radius, there is further acceleration of flow before the mid-section at $M_\infty = 0.6$ and $\alpha = 0^o$. This results in subsequent reduction in drag for the Busemann biplane. For the freestream Mach numbers between 0.6 and 0.9, this phenomenon of flow acceleration in the convergent and divergent portions of the biplane continues and the reduction in drag with increasing radii of leading and trailing edges is observed.

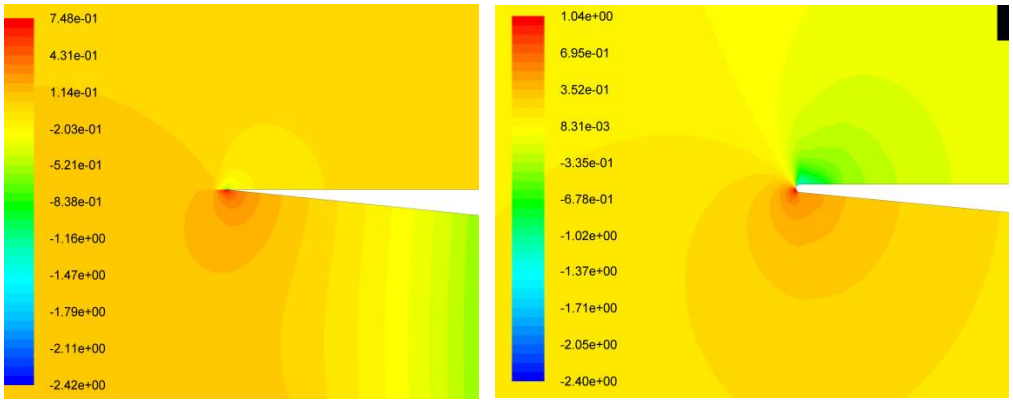

(a) ($C_D = 0.0627$) (b) ($C_D = 0.0618$)

Fig.: 5.21 C_P variation for Busemann biplane with a) sharp leading edge and b) rounded leading edge of 1 mm radius, at $M_\infty = 0.6$, $\alpha = 0^o$.

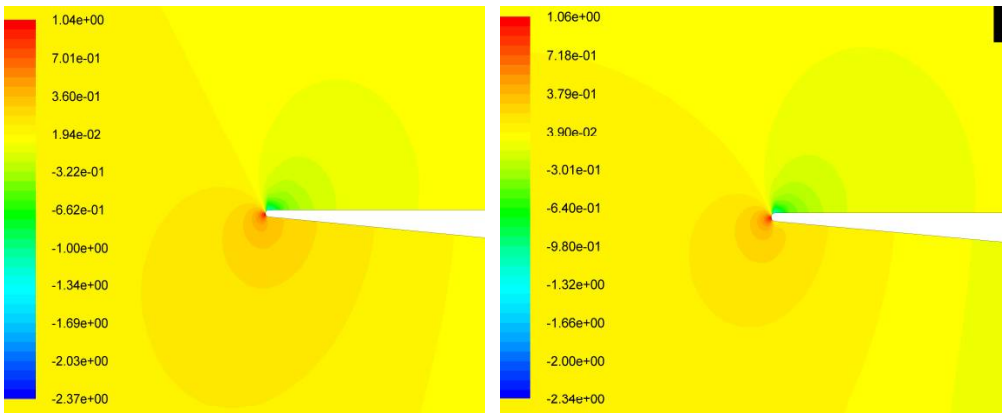

2mm Radius ($C_D = 0.0603$) 3mm Radius ($C_D = 0.0598$)

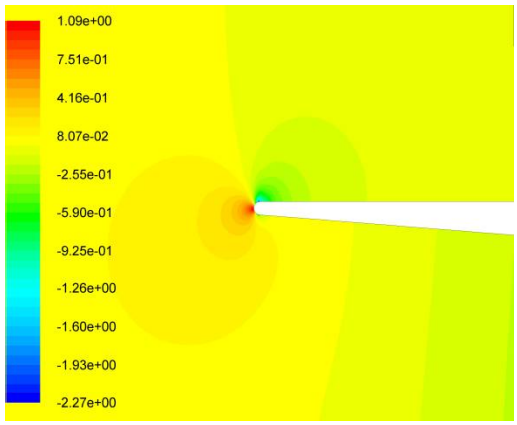

5mm Radius ($C_D = 0.0479$)

Fig. 5.22 C_P variation for different leading edge radius at $M_\infty = 0.6$, $\alpha = 0^o$.

For a freestream Mach number of 1 and higher but less than 1.7, the flow between the biplane elements becomes completely choked at the entrance itself. For these choked Busemann biplanes the pressure distribution on the inner surfaces becomes unaffected by the small geometrical variations at the leading and trailing edges. Typical pressure distributions near the leading edges of the biplanes with sharp end rounded leading edges for a freestream Mach number of 1, are shown in Fig. 5.23. Thus for freestream Mach numbers between $1.0 \leq M_\infty \leq 1.7$, the overall drag of the Busemann biplane is unaffected by the radius of the rounded leading edges. Due to the roundedness of the leading edge however, at supersonic speeds a detached shock wave is forms at the leading edge with a substantial rise in the stagnation pressure at the leading edge acting over a finite area of the leading edge. This results in slight increase in wave drag of the configurations but due to lower wave angles the pressure rise on the surfaces are slightly lower resulting in infinitesimal reduction in wave drag for rounded leading edge configurations.

For the freestream Mach number, $M_\infty \geq 1.7$, the flow chocking is eliminated and the flow aft of leading edge is supersonic, which induces an attached oblique shock at the sharp corner. At the blunt leading edge, due to a strong detached bow shock, the pressure near the blunt edge is more than the sharp edge as can be seen in Fig. 5.24 which shows the contours of pressure coefficients, near the leading edges, for various configurations with rounded leading edge at $M_\infty = 1.7$ and $\alpha = 0^o$. This results in an increased wave drag for configurations with rounded leading edges. As the radius of the leading edges is increased, the normal portion of the bow shock gets larger and larger with subsequent increase in the area over which the stagnation pressure acts. This also means an increase in the wave drag for Busemann biplane with increasing radius of rounded leading edge.

The rounding off of leading edge not only increases the extent of the stagnation region, but also modifies the shock-shock interactions between the elements as can be seen in Fig. 5.25.

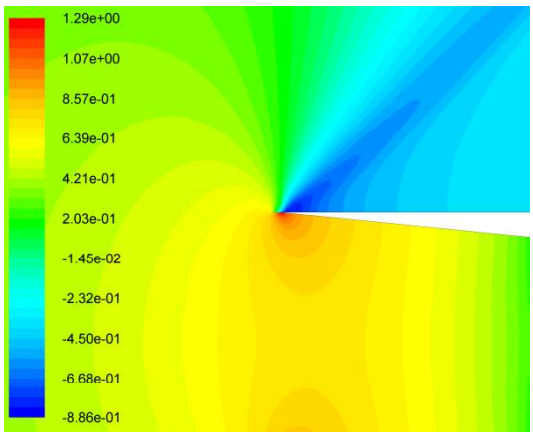

(a) Sharp Edge ($C_D = 0.1284$)

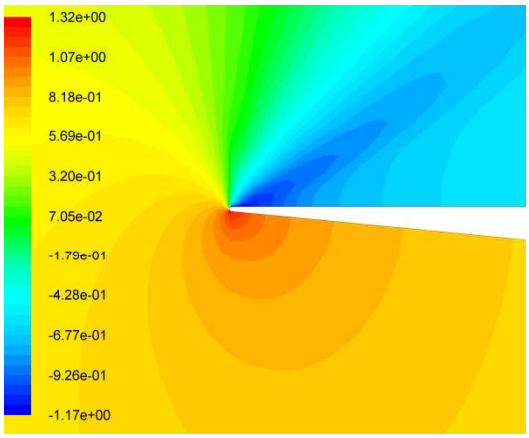

(b)1 mm Radius ($C_D = 0.1278$)

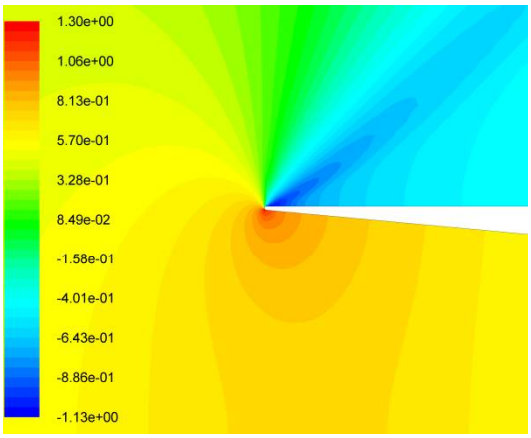

(c) 2 mm Radius ($C_D = 0.1278$)

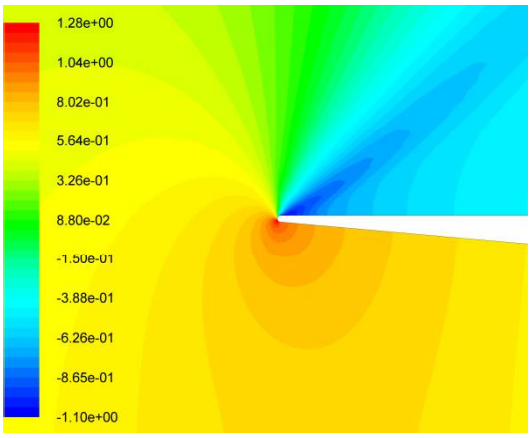

(d) 3 mm Radius ($C_D = 0.1274$)

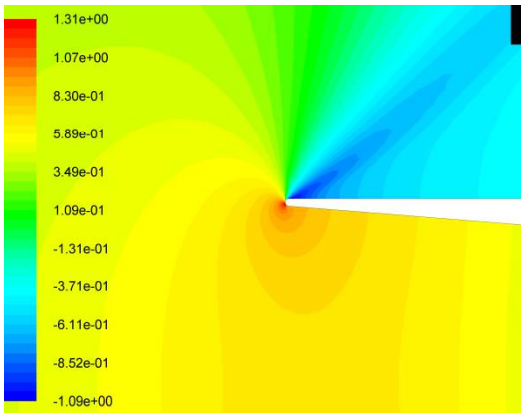

(e) 5 mm radius ($C_D = 0.1281$)

Fig. 5.23 C_p variation with leading edge radius at $M_\infty = 1$, $\alpha = 0^o$.

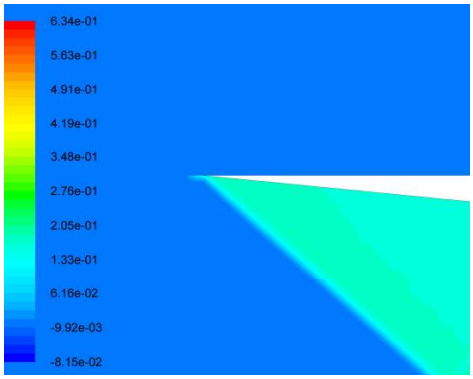

Sharp Edge (C_D = 0.00989)

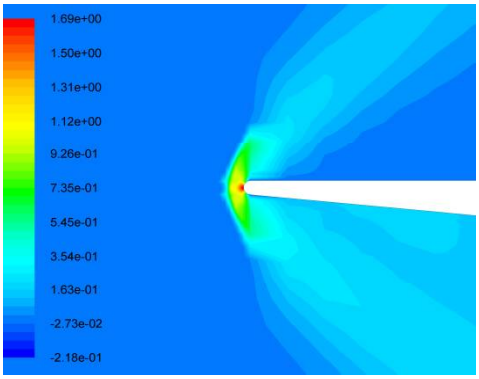

1mm Radius (C_D = 0.0140)

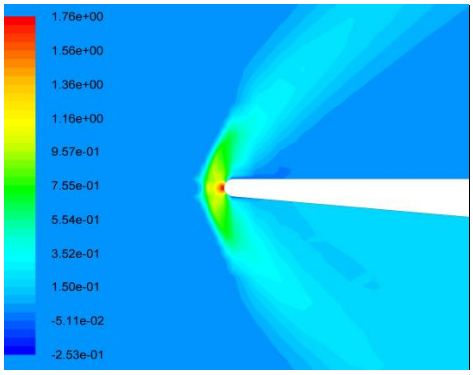

2mm Radius (C_D = 0.0186)

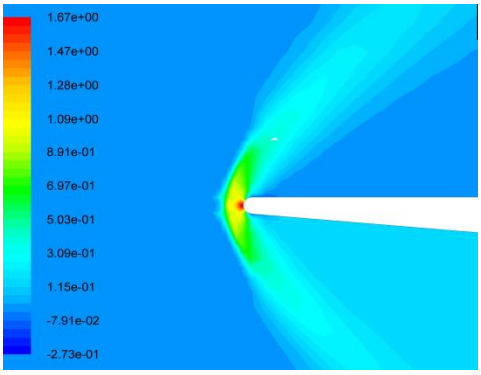

3mm Radius (C_D = 0.0233)

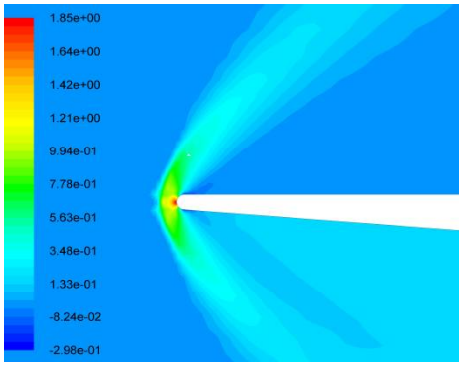

5mm Radius (C_D = 0.0330)

Fig. 5.24 C_p variation with leading edge radius at $M_\infty = 1.7$, $\alpha = 0^o$.

Fig. 5.25 shows the contours of pressure coefficients between the elements of Busemann biplane for a sharp leading edge and for a rounded leading edge with radius of 5 mm. As can be seen in Fig. 5.25, in case of sharp leading edge the attached shock waves interact with each other and impinges on the opposite element exactly at the point of maximum thickness from where the expansion

wave emanates. This results in a region of increased pressure near the throat area of the biplane. However, the pressure on the surfaces ahead and aft of the throat in slightly lower as compared to the diamond shaped high pressure region at the centre. In the case of rounded leading edge, strong bow shock waves are generated due to blunt leading edges which interact at a slightly forward position between the elements. This causes the oblique shock waves to impinge on the opposite elements at point much ahead of the throat and as a consequence the reflected shock waves cause an increased pressure on the inner surfaces ahead of the point of maximum thickness. With reduced pressure aft of the point of maximum thickness, the net result is an increased pressure drag as compared to the Busemann biplanes with sharp leading edges.

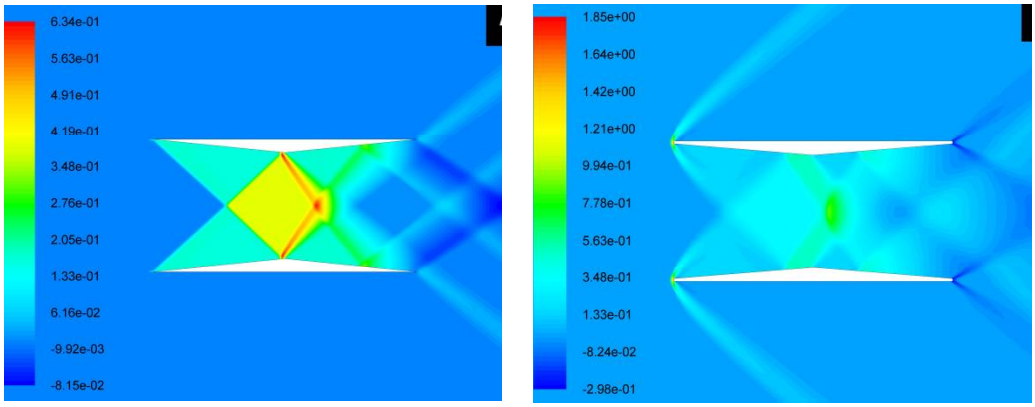

(a) Sharp leading edge (b) Rounded leading edge with 5 mm radius

Fig. 5.25: C_p variation of Busemann biplane at $M_\infty = 1.7$, $\alpha = 0^o$ for (a) sharp leading edge and (b)rounded leading edge with 5 mm radius

As the freestream Mach number is increased beyond 1.7 ($M_\infty > 1.7$), the strength of the bow shock wave ahead of the elements increases which in turn increases the wave drag for the combination. For very high supersonic Mach numbers some drop in the drag can be observed for both the configurations with sharp and blunt leading edges. This is because of the fact that the left and right running shock waves interact aft of the mid-section causing a higher surface pressure aft of the mid-section. the variation of drag coefficient, C_D with Mach number, M_∞ for different leading edge and trailing edge radius is shown in Fig. 5.26.

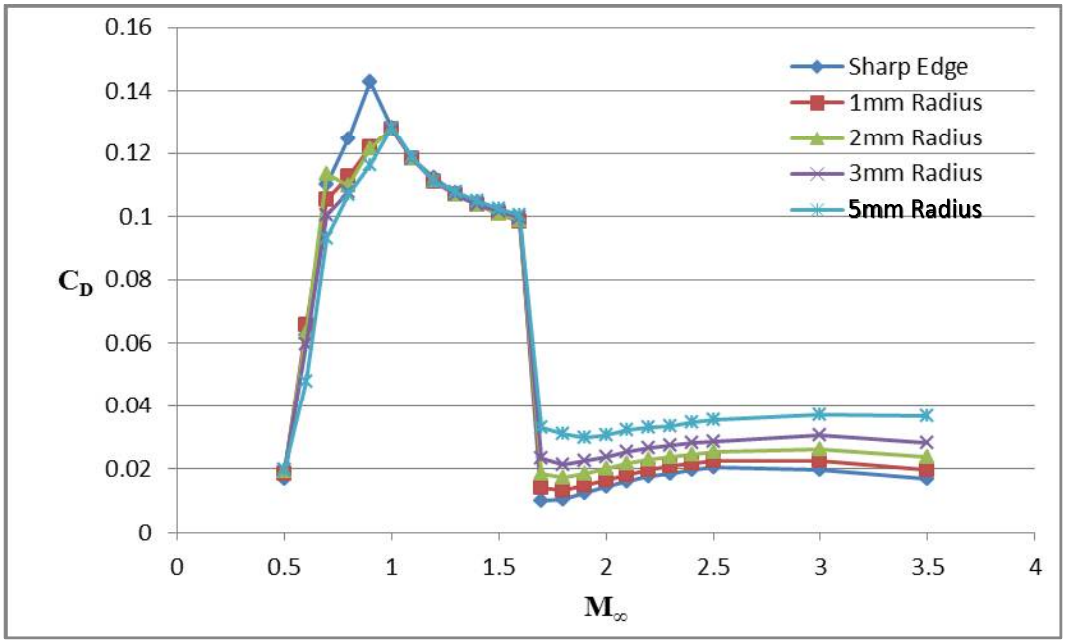

Fig.5.26: Variation of drag coefficient with leading edge and trailing edge radius for Busemann biplane at $\alpha = 0^o$.

5.4 Effect of Leading and Trailing Edge radii on Stagger biplane

The effect of rounded leading and trailing edges on the performance of staggered Busemann biplane element is also studied for different stagger distances of 0.1c, 0.2c, 0.3c, 0.4c and 0.5c and Mach numbers between 0.5 and 2.5. A typical multi-block structured grid around a staggered biplane with rounded leading and trailing edges is as shown in Figure 5.27.

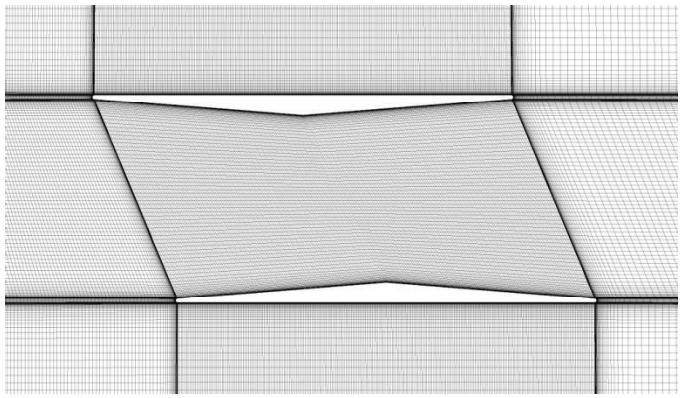

Fig. 5.27: Grid for staggered biplane with rounded leading edge and trailing edges

The effect of leading edge and trailing edge radii on aerodynamic characteristics of staggered biplane configuration is similar to that on the Busemann biplane. For subsonic freestream Mach numbers however, there is no change in drag for the staggered configurations with rounded leading edges as compared to the sharp edged configurations as can be seen in Fig. 5.28. For $M_\infty \leq 0.9$, no shock waves are formed at the leading edges and apart from a slight increase in stagnation area there is hardly any change in the flow field. Even for the Mach number in the range $1.0 \leq M_\infty \leq 1.7$, wherein the flow between the elements is choked, the flowfield is similar giving out similar values of drag coefficients. As can be seen in Fig. 5.26, apart from a curved detached bow shock for rounded leading edge, the entire flowfield and shock structure between the elements is similar. For the higher stagger of 0.4c and 0.5c two distinct bow shock waves are formed with substantial rise in stagnation pressure and a larger region of stagnation as can be seen in Fig. 5.28c. This is slightly different from the two oblique shock waves in in sharp leading edge configuration where the peak pressure coefficient is 1.01 as can be seen in Fig. 5.28d. This result in an increase in drag coefficients for staggered configurations with rounded leading edges as compared to sharp leading edges for a stagger of 0.4c or 0.5c at supersonic Mach numbers. At high supersonic Mach numbers greater than 1.7 the increased area of stagnation region and stagnation pressures due to distinct bow shocks continue to grow as can be seen in Fig. 5.28e. So the drag rise for supersonic flow is further strengthened as the Mach number is increased for all stagger as can be seen in Fig. 5.28.

As discussed in the previous paragraphs, for subsonic freestream Mach numbers the flowfield is only marginally modified by the rounding off of the leading and trailing edges. This means that the along with the drag, the lift of the staggered configurations is also not influenced by the rounded leading edges. This ensures that the aerodynamic efficiency, i.e. L/D ratio of the staggered biplanes remains unaffected by the rounding off of leading edges as can be seen in Fig. 5.30. Fig 5.30 shows the variation of L/D ratios with Mach numbers, for various staggered configurations with rounded leading edges of different radii.

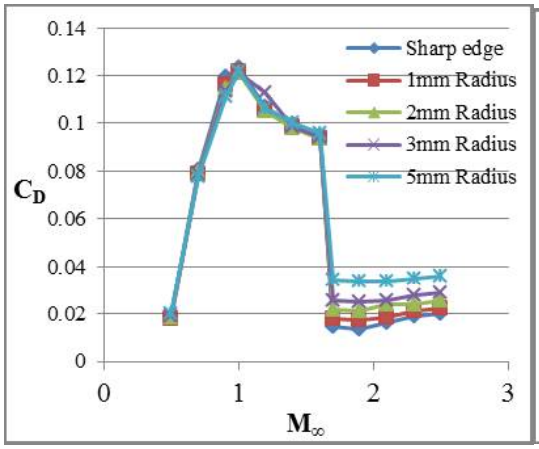

(a)Stagger =0.1c

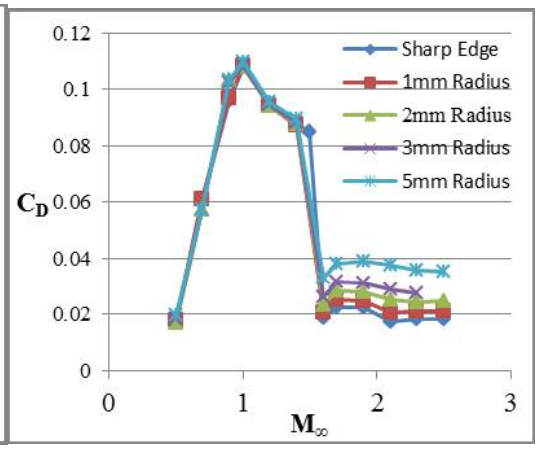

(b) Stagger =0.2c

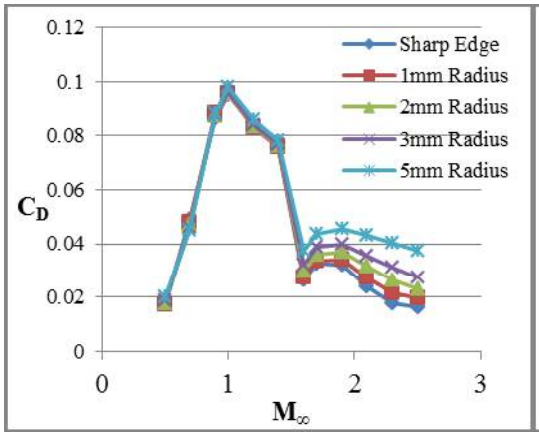

(c)Stagger =0.3c

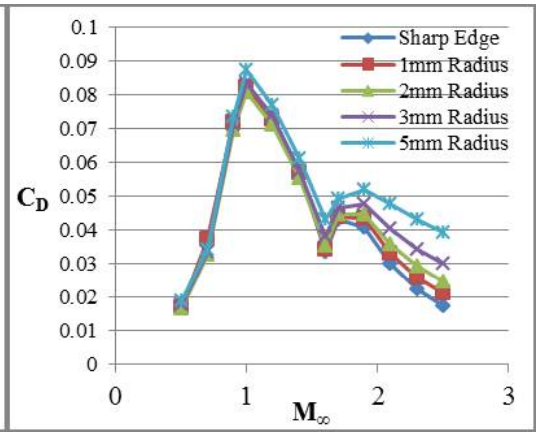

(d) Stagger =0.4c

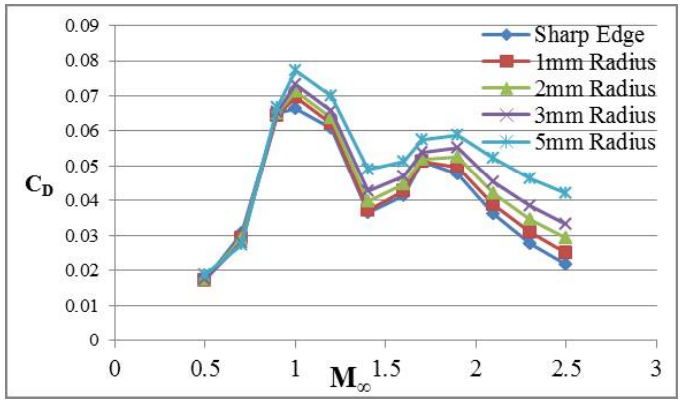

(e)Stagger = 0.5c

Fig. 5.28: C_D variation with M_∞ for radii of leading edge and trailing edges for stagger configuration at $\alpha = 0^o$.

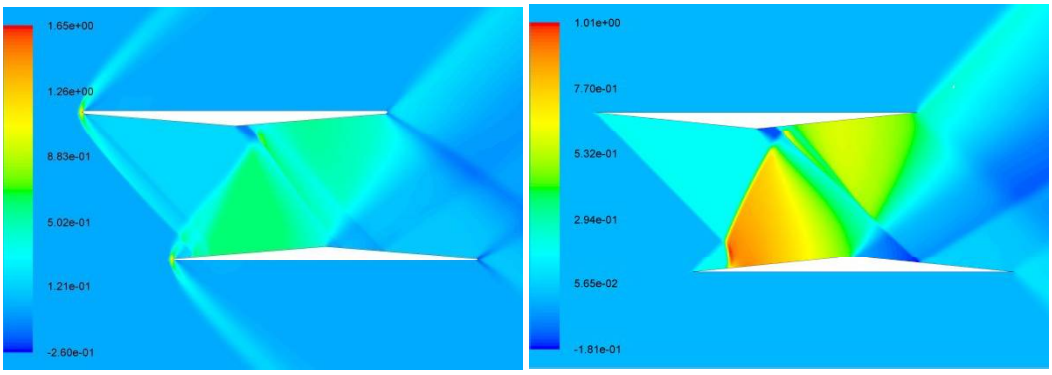

(a) Stagger 0.3c, M=1.6, radius=5 mm (b) Stagger 0.3c, M=1.6, sharp

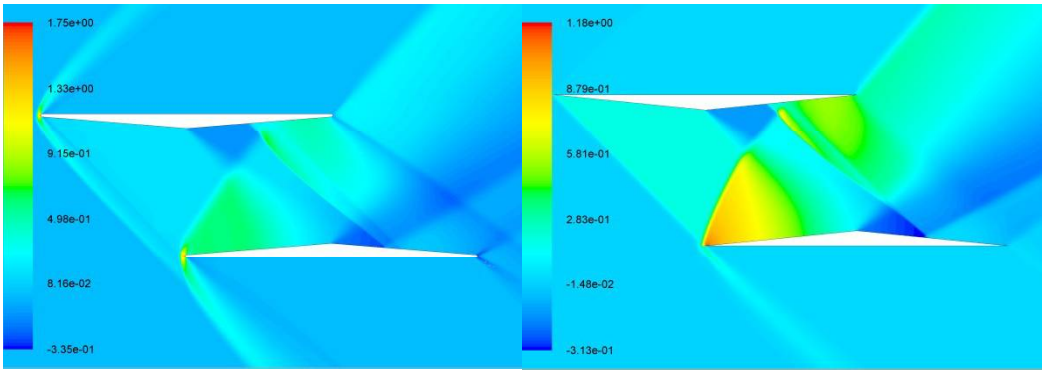

(c) Stagger 0.5c, M=1.6, radius=5 mm (d) Stagger 0.5c, M=1.6, sharp

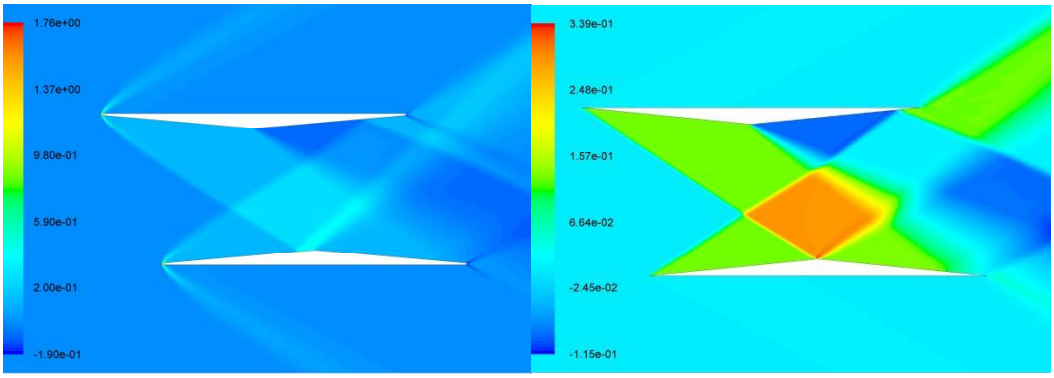

(e) Stagger 0.2c, M=2.1, radius=5 mm (f) Stagger 0.2c, M=2.1, sharp

Fig. 5.29: Comparisons of pressures contours for staggered configurations with round and sharp leading edges

For supersonic Mach numbers below the design Mach number of 1.7, although there is some modification in the flowfield, the modified field only affects a small portion of the elements at the leading edge. Thus the drag coefficients and the lift

coefficients are not influenced much giving overall *L/D* ratio similar to those for sharp edged configurations.

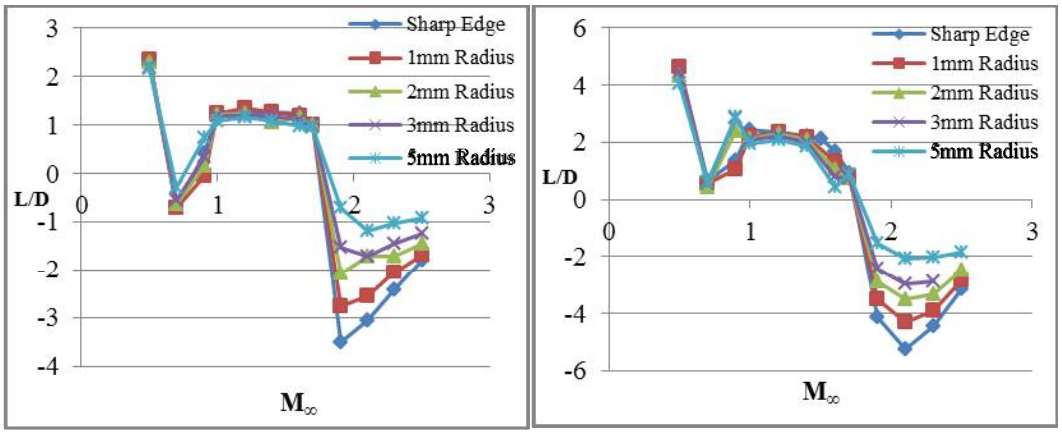

(a) Stagger 0.1c (b) Stagger 0.2c

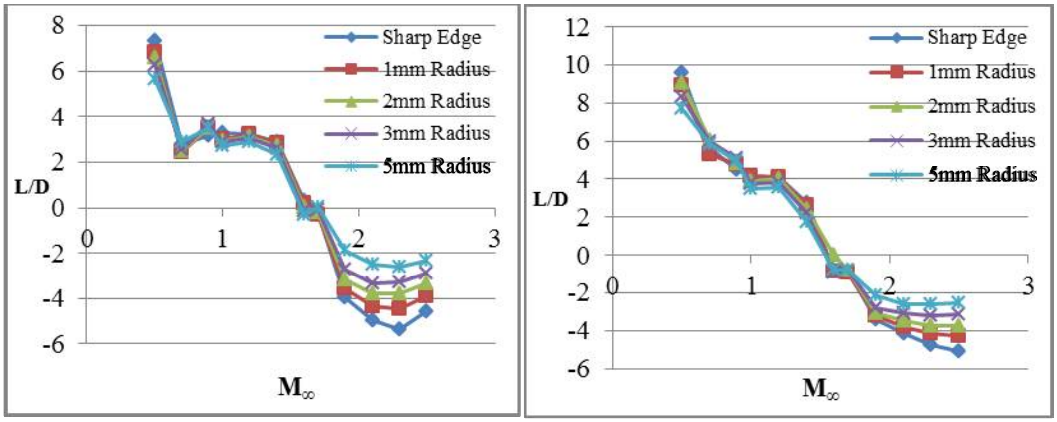

(c) Stagger 0.3c (d) Stagger 0.4c

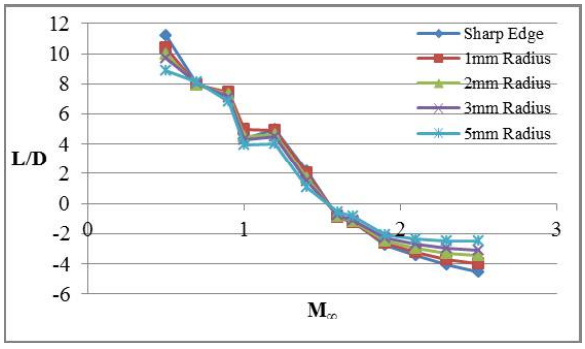

(e) Stagger 0.5c

Fig. 5.30: *L/D* variation with M_∞ for different leading and trailing edge radii for stagger configuration at $\alpha = 0^o$

For post design supersonic Mach numbers, a significant increase in drag because of strong bow shocks at the rounded leading edges causes the negative aerodynamic efficiency to improve slightly. The negative lift shown by the staggered configurations are eliminated as the angle of attack is increased. The roundedness of the leading edges eliminates the flow separation at small angles of attack in subsonic stream. This adds to the lift production and thus enhancing the aerodynamic efficiency of the staggered biplanes.

In summary the staggering of biplanes dramatically improves the aerodynamic efficiency of the biplanes at subsonic Mach numbers and at supersonic Mach numbers below design Mach numbers. Adding rounded leading and trailing edges to enforce structural strength does not seems to diminish the advantages of staggered biplanes at Mach numbers below the design Mach number of 1.7. The aerodynamic efficiency of the biplanes is slightly improved at sub-design Mach numbers with the use of rounded leading and trailing edges. This improvement comes primarily due to reduction in drag and a mild increase in lift at positive angles of attack. At supersonic Mach numbers above design Mach number, the roundedness of the leading and trailing edges causes a large increase in wave drag which deteriorates the performance of the staggered biplanes. Nevertheless, the staggered biplane configurations with rounded leading and trailing edges are suitable candidates for supersonic transport aircrafts to alleviate the sub-design Mach number performance as the airplane has to spend a lot of its mission time at subsonic Mach numbers.